Journal of Energy Storage 71 (2023) 108076

Contents lists available at ScienceDirect

Journal of Energy Storage

journal homepage: www.elsevier.com/locate/est

Research papers

# Experimental and computational optimization of eco-friendly mortar blocks for high temperature thermal energy storage of concentrated solar power plants

Irene Ramón-Álvarez [a], Sergio Sánchez-Delgado [b], Ignacio Peralta [c,d,e], Antonio Caggiano [f,*], Manuel Torres-Carrasco [a,*]

[a] University Carlos III of Madrid, Materials Sciences and Engineering Department-IAAB, Avda. Universidad 30, 28911 Leganés, Madrid, Spain
[b] University Carlos III of Madrid, Thermal and Fluids Engineering Department, Avda. Universidad 30, 28911 Leganés, Madrid, Spain
[c] Institut für Werkstoffe im Bauwesen, TU-Darmstadt, Darmstadt, Germany
[d] Centro de Investigación de Métodos Computacionales (CIMEC), UNL-CONICET, Predio CONICET "Dr. Alberto Cassano", 3000 Santa Fe, Argentina
[e] Laboratorio de Flujometría (FLOW), FRSF-UTN, Lavaise 610, 3000 Santa Fe, Argentina
[f] Dipartimento di Ingegneria Civile, Chimica e Ambientale - DICCA, Università degli Studi di Genova, Via Montallegro, 1, 16145 Genova, Italy

ARTICLE INFO

*Keywords:*
Alternative binders
Alkaline mortars
Hybrid mortars
Solar thermal energy
Concentrated solar power technologies
Numerical simulations
Experimental analysis

ABSTRACT

New avenues for thermal energy storage (TES) need to be investigated due to the lack of competitiveness of concentrated solar power (CSP) technologies. Solutions must be found to replace molten salt tanks which have a major economic impact and are difficult to maintain due to corrosion problems. In this sense, concrete represented an attractive candidate by proving excellent sensible TES in CSP. However, its main phase, made of Portland cement (PC), has significant environmental consequences. The production of PC is known to emit high levels of polluting gases, particularly the $CO_2$. It is estimated to be responsible for between 5% and 7% of the world's $CO_2$ emissions, making it a major contributor to climate change. This work presents greener cementitious materials, made of alkaline cements and hybrids cements, to be used as alternative eco-friendly TES media in CSP plants. An experimental campaign is presented which shows that these eco-efficient materials can have better mechanical properties, than the ordinary PC mortar, when exposed to high temperatures, in addition, can offer improvements of their thermal properties (thermal conductivity or specific heat). Second part of the work is devoted to Finite Element simulations, with the aim to find the best configuration, in terms of selection of materials and geometry, which are more efficient as TES system. The work is showing the following advancements in CSP technology by using alternative eco-friendly binders: the installation volume can be reduced by 17%, compared to a molten salt tank, while the heat exchanger's surface area can be resized by 29%, compared to the reference system using PC. These improvements enable wider variations in CSP operational efficiency and dynamic capabilities and represent important progress towards developing more efficient and sustainable CSP technologies.

## 1. Introduction

In the last Climate Change Conference (COP27), it was agreed the acceleration of actions related to reduce the $CO_2$ emissions, the removal of inefficient fossil subsidies and the promotion of renewable energies [1]. Renewable energies allow a significant reduction of $CO_2$ by avoiding the use of fossil fuels. However, even though there has been a growth of these technologies, renewable energies must need an improvement in their energy efficiency due to the transient variability of the energy source (e.g., wind, sun, etc.) which specially causes a mismatch between the energy supply and demand. One way to mitigate this problem is through a smart usage of energy storage systems that lead to important cost savings [2–7]. Due to climate change and air pollution, as well as to compliance with legislative regulations and specific credits for "green" electricity, there is an increasing interest in thermal energy storage (TES) for concentrated solar power (CSP) plants. Their implementation leads to an increase in the annual contribution of solar-based renewables, an improvement in the efficiency of the plants and a reduction of

* Corresponding authors.
*E-mail addresses:* antonio.caggiano@unige.it (A. Caggiano), matorres@ing.uc3m.es (M. Torres-Carrasco).

https://doi.org/10.1016/j.est.2023.108076
Received 23 March 2023; Received in revised form 21 May 2023; Accepted 13 June 2023
Available online 30 June 2023

the levelized cost of energy (LCOE) [8].

It is important to focus on the solar annual contribution since CSP technologies are not competitive technologies even in the sunniest locations from an economical and efficiency point of view. Their costs are determined, among other things, by the TES systems currently in use, which classically consist of two metal tanks tank filled up with molten salts. The combination of the molten nitrates (mainly used as heat transfer fluid-HTF, made of $NaNO_3$ in 60 wt.% and $KNO_3$ in 40 wt.% mix, commonly known as Solar Salt) with metal tanks generates a system with high cost due to the need of use of highly-expensive Ni-based superalloys, or austenitic stainless steels, to avoid corrosion problems [9]. In addition to the expensive materials used for the tanks, there are other aspects that need to be improved: the high risk of solidification due to the high freezing point of molten salts, a relatively small temperature difference between the hot and cold fluid in the TES, which decreases the dynamics of the CSP plants, and losses in the solar field due to the high outlet temperature, resulting in more expensive pipes and materials [3]. However, not only operational characteristics must be considered; it has been observed that the steel installation (tanks and piping circuit), together with the molten salts, account for 69.3% of total $CO_2$ emissions in a CSP plant. Focusing only on the TES medium, it is described that for 1 kg of molten salts produced, >6.5 kg of CO2 are emitted [10].

For these reasons, new TES systems are being studied to boost CSP plants. Specifically, cheaper TES (which can reduce the cost of the TES system by at least 35%) to guarantee the future success of CSP technologies are worth to be investigated [11,12]. Thermal energy can be stored in three ways: by sensible heat storage, latent heat storage and chemical heat storage. Sensible heat storage is the simplest one [4,6], and very attractive in terms of investment and maintenance costs [13]. In this context, one of the most attractive solid which provides a viable option to operate as TES in this way is concrete [14–16]. Concrete is chosen because of its low cost, high availability, and ease of production. It is a material that has high specific heat, so it keeps heat for longer time and allows to reduce the storage volume. In addition, it has good mechanical properties and can maintain them after it's exposed to thermal cycles. However, its main disadvantage is related to its quite low thermal conductivity, which is the main reason why large heat exchangers (with high investment cost) are required to transfer the thermal energy to/from HTF. As it can be seen in Fig. 1, concrete-based heat exchangers are based on metal tubes which are embedded in the concrete to let the HTF flows through them transferring its heat to the concrete (during the charging process) and taking the heat from the concrete (during the discharging process). The tubes are made of steel whose coefficient of thermal expansion (CTE) is similar to that of concrete, which allows the TES system to maintain high cycling stability over a long period of time [3,13,17].

CSP concrete was tested on a large-scale using blocks with embedded steel pipes to study its feasibility [14], resulting in good mechanical properties after exposure to 500 °C, and also after thermal cycles in the range of 200 °C to 400 °C, typical operational temperatures for this cementitious materials [5]. These described temperatures, although

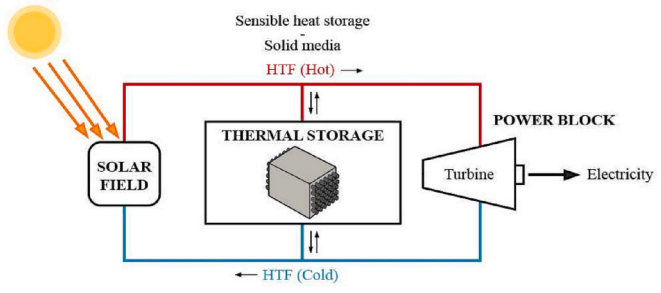


**Fig. 1.** Operation of a CSP plant with sensible heat storage based on a concrete block with embedded steel-based pipes.

commonly used in the application, represent the maximum limit that the concrete can face. In the case of molten salts, it is true that this limitation does not exist, since, for example, nitrate salts are capable of reaching almost 600 °C [5]. Even though the operational temperature limit is lower, it has been concluded that concrete really fits as a TES system as it can offer high power levels during the discharge, due to the integrity exhibited when a large temperature difference is established between the block and the HTF [15]. It is demonstrated in literature that concrete, as a sensible storage, shows an improvement in the overall performance of CSP technology when compared to the conventional two-tank, indirect, molten salt TES [16]. Concrete proves to be a fully scalable technology that can be installed anywhere [18]. Its viability as TES system has already been tested also on small-scale in the laboratory or by using Finite Element Method (FEM) analysis and CFD codes by several researchers [8,13,19–30].

Computational modelling allows an easy optimization of TES blocks without spending material resources and time on designing complex experiments. FEM allows pre-calculations and design objectives that can indicate which system offers the best thermal behavior (determining materials, geometry and arrangement of the pipes in the block, number of heat exchangers) for its subsequent fabrication [19,30]. TES designs must be carefully optimized to provide storage and release operating times compatible with commercial applications [20]. Another technical point of view to be taken into account is the amount of stored energy in the block and also, the one that can be supplied [11], since the stored thermal energy is the main key to determine the viability of a system such as TES [23]. The efficiency of the storage unit can be improved by increasing the operational temperatures, which can be optimized according to the used materials [23]. Block efficiency has to take into account not only the operational parameters, but also costs, since, as it was explained before, CSP technology could be not as competitive from an economic point of view [9].

The costs of a sensible heat storage depend on the material, the cost for the space and the enclosure for the TES (as both molten salts and cementitious materials need to be located in an insulated container to prevent heat losses), and the heat exchangers (embedded pipes) [11,16,31]. Among these three elements, embedded metal tubes stand out or their higher cost [13,21–23], which can account for >50% of the total TES price [11]. An improvement in the performance of the block has been demonstrated by inserting multiple heat exchangers (pipes) into the TES [26,32] but its optimization should always be considered (pipe diameter, number of pipes, arrangement of the pipes in the block, etc.) in order to achieve maximum transfer energy (heat exchangers have a greatly influence in charging/discharging times) without neglecting the economic impact [8,21,27,28]. Another way to save costs, in addition to the heat exchanger optimization, is based on finding the way to reduce the TES installation space by getting a block material that can store more energy [23].

In this context, concrete is very convenient because of its low price, besides of its good skills to be a promising TES media in CSP as TES. However, the fabrication of its main raw material, Portland cement (PC), has a high and negative environmental impact. PC industry contributes detrimentally to the environment since consumes a large sum of fossil fuel, being 12–15% circa of the total industrial energy consumption [33]. In addition, polluting gases are emitted during PC production, accounting the cement industry for 5–7% of the $CO_2$ global emissions (it is estimated that for every ton manufactured of PC, up to one ton of $CO_2$ is emitted) [34,35]. Thus, in ecological terms, it is not an alternative to molten salts. In addition, it has also been found that concrete has a high water footprint impact since water is an element which is needed in almost every step of its production [36].

Because of those disadvantages, two alternatives were developed: the use of alkali-activated materials (AAM), so-called geopolymers, and the hybrid materials (HM).

AAM can fully substitute PC using aluminosilicate materials (that can be natural minerals or by-products of industrial processes). They need to

be activated with high pH alkaline solutions that limit the workability in the construction sector [37,38]. To avoid that type of activators, HM emerged. HM reduces the amount of PC as it is employed in a low content (20–30%). Then, the main precursor, as in the case of the AAM, is an aluminosilicate material (70–80%) which is activated with soft alkaline salts (commonly used in a solid state) just in presence of water [39]. A significant cost reduction together with environmental improvements can be achieved when by-products are used in cementitious materials, since are waste from other industries that otherwise would end up in dumps, and their recycling leads to a decrease in the energy needed in the manufacturing process [33,40–44]. By-products can be used not only as a part of the binder (substituting PC) but also, as a part of the aggregate, substituting the natural aggregate (NA) (sand), to avoid abiotic depletion, eutrophication, acidification [45] and $CO_2$ emissions [46], among other environmental problems.

Considered the serious environmental drawbacks of PC and sand mentioned above, this study proposes the development of new alternatives to continue exploring the advantages of construction materials as TES media employed in CSP plants. Thus, AAM and HM systems were manufactured following the principles of the circular economy using waste and industrial by-products.

Numerical and experimental studies have been carried out to test their feasibility as a TES. Thermal cycles were performed to test the stability of the mortars between 200 °C and 400 °C, as the operational temperatures in parabolic trough collectors (the most common CSP technology in the 95% of the cases) vary from 290 °C to 390 °C and also, because concrete as sensible heat storage has been shown to be stable in these temperature ranges [5,8,17]. After 20 thermal cycles, mechanical properties were studied by compression tests. Then, density, specific heat and thermal conductivity of the materials were measured to use them as input parameters in a FEM simulation. The numerical tests were done to optimize firstly the design of the blocks (obtaining a system that provides a faster heating [13]) and then, to study which mortar has a better operational performance in a CSP, considering technical and economic variables. The comparison between systems was made considering a stored energy of 1100 MWh, which is the energy stored today in tanks of molten salts in a 50 MWel parabolic trough power plant of ANDASOL (taking into account full charge and discharge cycles, i.e. during 7.5 h of storage) [14].

## 2. Experimental procedure

### 2.1. Materials

Three types of mortars were performed (a reference sample, made of and referred as PC; an AAM, referred as SLAG, and a HM, referred as HSLAG). For them, two binders were used: Portland cement I 42.5R, supplied by the company "*Cementos Portland Valderrivas*", and an industrial by-product, a blast furnace slag from ENSIDESA (Avilés, Spain). Sand (S) was substituted in percentage by weight with glass waste (GW) from "Ecovidrio" (Ajalvir, Spain). The particle size of the used GW was under 2 mm to resemble the material that was replaced. To achieve that particle size, GW was ground by using a cross beater mill.

The chemical compositions of the different raw materials (Portland cement and blast furnace slag) and the recycled aggregate (GW) are shown in Table 1, where it can be observed that the content of CaO, $SiO_2$ and $Al_2O_3$ is the majority in PC and SLAG. Regarding the GW, its main component is $SiO_2$.

### 2.2. Sample preparation

All mortars have been prepared under the UNE EN 196-1 [47] standard:

- PC mortar: Portland cement CEM I 42.5R and aggregate (ratio 1:3 respectively) hydrate just in presence of water.
- SLAG mortar: blast furnace slag and aggregate (1,3 ratio) were used. It was activated with a commercial solution of sodium silicate (waterglass) that was diluted with water and NaOH to achieve a $SiO_2/Na_2O$ ratio equal to 0.8.
- HSLAG mortar: the mix is based on a 77.5% weight of slag and 17.5% weight of CEM I 42.5R. In addition, the HM systems contain a soft alkaline activator, specifically, 5% of $Na_2SO_4$ was added to accelerate the hydration process that it is produced with water [48]. These systems were also prepared with a precursor/aggregate ratio of 1:3.

The NA (sand) was substituted by glass waste (GW) as previous studies demonstrated its high impact on the water footprint [36]. The substitution of sand by GW in weight percentage was 25%, 50%, 75% and 100%. To provide the same workability in all systems, the liquid/solid (L/S) ratios were varied following the UNE EN 1015-6 standard [49]. Table 2 shows the exact quantities of each component to manufacture the different systems. The mortar was poured into rectangular molds (4 × 4 × 16 cm) after the mixing in an automatic laboratory mixer. To improve the mortar distribution in the rectangular mold, the Proeti automatic compactor was used according to the UNE 196-3 standard [50]. The mortars were then cured for 28 days in a humid climate container (99% relative humidity) at room temperature (22 °C) before they were tested.

### 2.3. Equipment and procedure

To study the viability of the materials as TES, thermal cycles were performed between 200 °C and 400 °C with heating/cooling ramps of 6 °C/min to ensure high thermal stress under real condition [7]. The minimum and maximum temperature (200 °C or 400 °C) were maintained for 40 min to ensure temperature homogeneity at all points of the mortar [51]. The temperature range was selected because these are the optimum temperatures at which concrete can operate [5,17] and also, because CSP technology usually operates between 290 °C and 390 °C [8]. The exposure was defined at 20 cycles because the decrease in mechanical properties compared to those obtained after the first thermal cycle (when water evaporates and can lead to crack formation and thus to an increase in porosity [52]) was not significant and also, because there is very little information in the literature on the effects of thermal cycling on cementitious materials to be used as TES [7]. Given the critical process of water evaporation, a previous heat treatment was carried out to slowly remove the water to avoid the spalling phenomenon. The samples were subjected to a heating ramp at 2 °C/min and were exposed to 100 °C during 24 h [53].

Then, different tests were carried out on untreated samples and those exposed to 20 cycles:

**Table 1**
Chemical composition of the raw materials (wt.%) by XRF.

| wt.% | CaO | $SiO_2$ | $Al_2O_3$ | MgO | $Fe_2O_3$ | $SO_3$ | $Na_2O$ | $K_2O$ | LoI[a] |
|---|---|---|---|---|---|---|---|---|---|
| Portland cement | 61.94 | 21.28 | 6.45 | <0.003 | 2.53 | 5.87 | <0.012 | 1.01 | 2.35 |
| Blast furnace slag | 35.73 | 36.15 | 11.75 | 12.75 | 0.38 | 1.75 | <0.010 | 0.27 | 2.10 |
| GW | 11.75 | 70.71 | 2.05 | 1.17 | 0.52 | – | 11.71 | 1.08 | 0.83 |

[a] LoI: loss on ignition.

**Table 2**
Mortar preparation.

| Nomenclature | Raw material (g) | Addition | L/S | Water (g) | Activator solution (g) | Aggregate (g) |
|---|---|---|---|---|---|---|
| PC 100 S | 450-PC | – | 0.50 | 225-$H_2O$ | – | 1350-S |
| PC 75 S | 450-PC | – | 0.57 | 256.5-$H_2O$ | – | 1012.5-S<br>337.7-GW |
| PC 50 S | 450-PC | – | 0.60 | 270-$H_2O$ | – | 675-S<br>675-GW |
| PC 25 S | 450-PC | – | 0.62 | 279-$H_2O$ | – | 337.7-S<br>1012.5-GW |
| PC 100 GW | 450-PC | – | 0.64 | 288-$H_2O$ | – | 1350-GW |
| SLAG 100 S | 450-SLAG | – | 0.55 | – | 247.5-$Na_2SiO_3$ Solution | 1350-S |
| SLAG 75 S | 450-SLAG | – | 0.54 | – | 243-<br>$Na_2SiO_3$ Solution | 1012.5-S<br>337.7-GW |
| SLAG 50 S | 450-SLAG | – | 0.65 | – | 292.5-$Na_2SiO_3$ Solution | 675-S<br>675-GW |
| SLAG 25 S | 450-SLAG | – | 0.73 | – | 328.5-$Na_2SiO_3$ Solution | 337.7-S<br>1012.5-GW |
| SLAG 100 GW | 450-SLAG | – | 0.76 | – | 342-<br>$Na_2SiO_3$ Solution | 1350-GW |
| HSLAG 100 S | 348.75-SLAG; 78.75-PC;<br>22.5-$Na_2SO_4$ | 5% $Na_2SO_4$ | 0.46 | 207-$H_2O$ | – | 1350-S |
| HSLAG 75 S | 348.75-SLAG; 78.75-PC;<br>22.5-$Na_2SO_4$ | 5% $Na_2SO_4$ | 0.48 | 216-$H_2O$ | – | 1012.5-S<br>337.7-GW |
| HSLAG 50 S | 348.75-SLAG; 78.75-PC;<br>22.5-$Na_2SO_4$ | 5% $Na_2SO_4$ | 0.51 | 229.5-$H_2O$ | – | 675-S<br>675-GW |
| HSLAG 25 S | 348.75-SLAG; 78.75-PC;<br>22.5-$Na_2SO_4$ | 5% $Na_2SO_4$ | 0.55 | 247.5-$H_2O$ | – | 337.7-S<br>1012.5-GW |
| HSLAG 100 GW | 348.75-SLAG; 78.75-PC;<br>22.5-$Na_2SO_4$ | 5% $Na_2SO_4$ | 0.58 | 261-$H_2O$ | – | 1350-GW |

- Microtest universal testing machine, with the 200 kN load cell to register the necessary force to cause the compression failure of the mortar, was used to carry out the compression tests. Five repetitions were carried out for each type of mortar.
- MP-2 Thermal Conductivity Measurement Platform, using the TLS 50 mm sensor was used to measure the thermal conductivities (ten repetitions per mortar) before and after the exposure of mortars to thermal cycles. To be able to insert the sensor, the mortars were previously drilled with a vertical drill.
- Specific heat of the mortars was analyzed by differential scanning calorimeter (DSC) equipment, model 822 (Mettler Toledo GmbH, Greifensee, Switzerland). Mortars were ground and 15 mg powder were placed into aluminum crucibles of 40 µl. Samples were heated in the temperature range of 0–400 °C and nitrogen (35 ml/min flow) was used as purge gas. Two ramps were performed from 0 to 400 °C

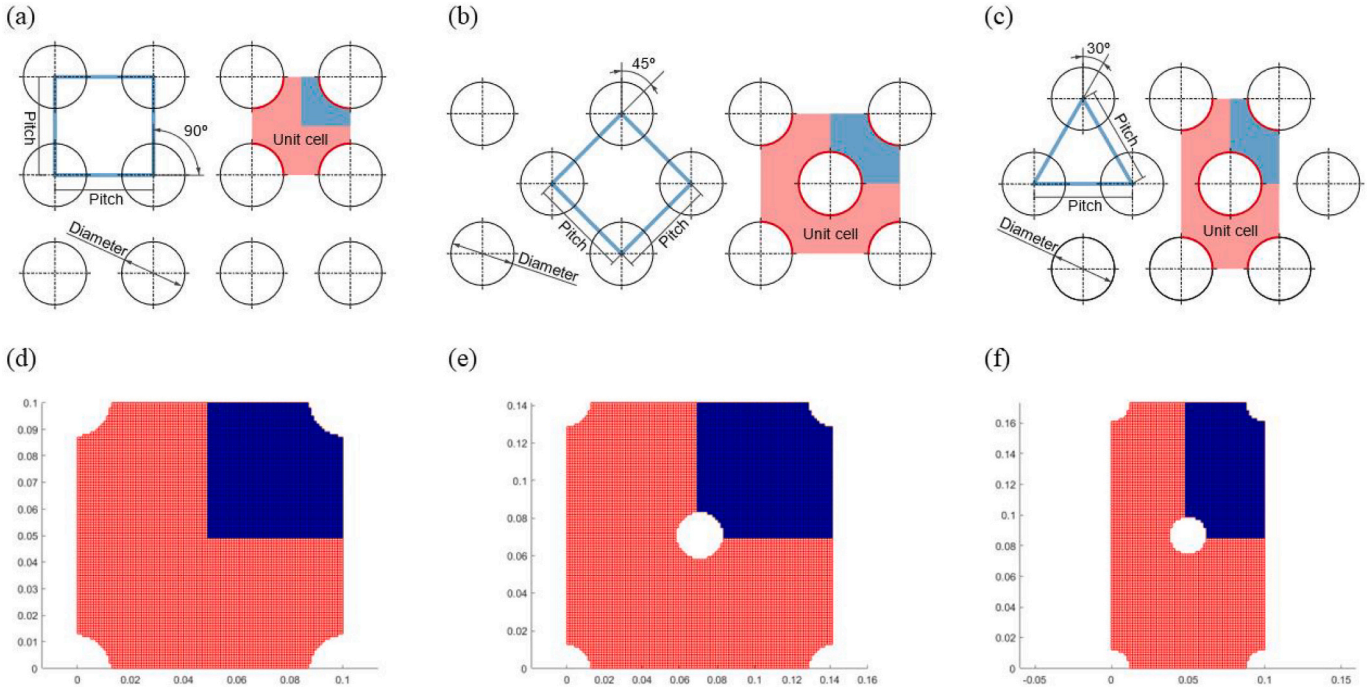


**Fig. 2.** (a) (b) (c) Unit cell arrangements with their main parameters. (d) (e) (f) Geometry and considered mesh studied in the simulation: (a, d) Square arrangement with a 90° angle; (b, e) Triangular distribution with an angle of 45°; (c, f) Triangular distribution with an angle of 30°.
The blue area represents the points that provide the average temperature of the quarter of the block. (For interpretation of the references to color in this figure legend, the reader is referred to the web version of this article.)

to calculate Cp after the complete evaporation of water. The heating rate was established at 10 °C/min and liquid nitrogen was used to cool the samples. Three different measurements were carried out to obtain an average.

- ACCUPYC 1330 helium pycnometer (Micromeritics, Norcross, GA, USA) was used to measure the theoretical density ($\rho_t$) with gas displacement. Bulk density ($\rho_b$) was calculated by Archimedes principle following the UNE-EN 993-1:2018 standard [54]. With theoretical and bulk densities (three measurements of each one in the different mortars), total porosities ($\pi_t$) were calculated using Eq. (1):

$$\pi t\ (\%) = \frac{\rho t - \rho b}{\rho t} 100 \tag{1}$$

## 3. Finite element modelling

To investigate the charging/discharging behavior of the mortars, numerical simulations based on FEM were carried out. These simulations considered a unit cell, which is representative of the minimum portion of a TES block geometry when repeated in both the x and y axes. The three classic arrangements of the unit cell that were considered in a heat exchanger [55] are shown in Fig. 2 a–c. They represent i) the square arrangement with a 90° angle, ii) the triangular distribution with an angle of 45° and iii) the triangular distribution with an angle of 30°.

The unit cell makes it possible to study the optimal and most efficient arrangement of pipes, together with their diameter and pitch. This portion is representing a 2D section taken out from a 3 × 3 × 21(x, y, z) $m^3$ mortar block, whose dimensions follow the size of previous studies [14]. Thanks to the symmetry, the average temperature given by a quarter of the block (represented in blue in Fig. 2 a–c) was studied.

The unit cell is adiabatic at its borders, meaning there is no heat exchange with the surroundings. This is due to the periodic behavior of all adjacent cells, where there is no heat exchange between them. Then, the block is heated by a HTF that flows through the pipes at a charging temperature of 390 °C. The problem is simplified by assuming that the wall of the pipe is directly at 390 °C (no internal flow considerations are made). In the opposite case (the discharge case) the temperature of the pipe is 290 °C.

### 3.1. Governing equation

Following the basic equations that describe a heat conduction problem and based on the Enthalpy and Apparent Calorific Capacity Method (ACCM), which is the most widely used method for solving TES processes in cement-based materials [56], Eq. (2) is obtained to describe the temperature field $T$ in the domain Ω of Fig. 3

$$\rho_c c_c \frac{\partial T}{\partial t} - \nabla \cdot (\mathbf{k} \nabla (T)) = q, \tag{2}$$

subject to the boundary conditions (B.C.)

$$\text{Dirichlet B.C.} : T = T_{wall} \forall \mathbf{x} \in \partial\Omega_T \text{ and } t > 0, \tag{3b}$$

$$\text{Neumann B.C.} : -\mathbf{k} \nabla T . \mathbf{n} = 0 \forall \mathbf{x} \in \partial\Omega_q \text{ and } t > 0, \tag{3c}$$

and initial condition

$$T = T_0 \forall \mathbf{x} \in \Omega \text{ and } t = 0, \tag{3d}$$

being $t$ the time, $\mathbf{k}$ the effective thermal conductivity tensor of the material (depending on the position vector $\mathbf{x}$ of the considered body Ω), $q$ the possible source term, ∇. and ∇ the divergence and gradient tensorial operators, respectively, $T_{wall}$ the charging or discharging temperature (i.e., 390 or 290 °C, respectively), $\mathbf{n}$ the unit vector normal to and pointing outwards $\partial\Omega_q$, and $T_0$ the initial temperature of the block equal to 290 °C, if the unit cell is to be heat, or the maximum heating temperature reached for each distribution (almost 390 °C), if the discharging process is carried out.

In this work, the heat transfer problem only considers a sensible-based process and assumes a constant value of heat capacity $\rho_c c_c$.

### 3.2. FEM discretization

The temperature field $T$ in the domain Ω of Fig. 3 is discretized in the finite element domain assuming the interpolation strategy (Eq. (4))

$$T = \mathbf{N} \cdot \mathbf{T} \rightarrow \nabla (T) = \nabla (\mathbf{N} \cdot \mathbf{T}), \tag{4}$$

where $\mathbf{N} = [h_1, h_2, \ldots, h_n]$ is the set collecting the shape functions, and $\mathbf{T} = [T_1, T_2, \ldots, T_n]^t$ the nodal temperatures (unknown) of a mesh having $n$ nodes.

Using a standard (Galerkin) FEM, the set $\mathbf{T}$ is the solution of the algebraic system of equations (discretized version of the problem of Eqs. (2) + (3c))

$$\mathbf{C} \cdot \dot{\mathbf{T}} + \mathbf{K} \cdot \mathbf{T} = \mathbf{F}_Q + \mathbf{F}_q = \mathbf{0}, \tag{5}$$

being $\mathbf{C}$ and $\mathbf{K}$ the global constitutive matrices (capacity and conductivity, respectively), while $\mathbf{F}_Q$ and $\mathbf{F}_q$ the assembled global vectors, whose values are zero since no heat sources neither non-zero Neumann boundary condition are considered in this study, and $\dot{\mathbf{T}}$ is the set containing the time derivative of the nodal temperatures on the global reference system (for more details regarding the solution of the FEM

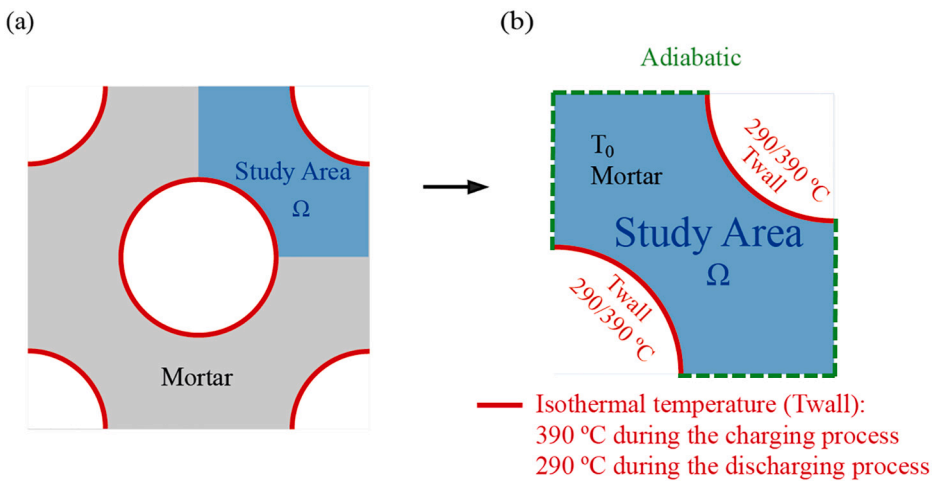


**Fig. 3.** (a) Domain of analysis (b) Study area conditions.

problem, see for instance the book of Zienkiewicz and Taylor on the basics of FEM [57]).

### 3.3. Time integration

Let us discretize the time domain $[0, t_N]$ in $N$ time steps $[t_n, t_{n+1}]$, with:

$$0 = t_0 < t_1 < t_n < t_{n+1} < \ldots < t_{N-1} < t_N, \tag{6}$$

being $t_N$ the total time. Then, by using the finite difference approximation of time-derivative for $\dot{\mathbf{T}}$:

$$\dot{\mathbf{T}} = \frac{\mathbf{T}_{n+1} - \mathbf{T}_n}{\Delta t}, t_n < t < t_{n+1} = t_n + \Delta t. \tag{7}$$

Now, by applying the theta-method for time integration, Eq. (5) at the time instant $t_{n+\theta} = \theta t_{n+1} + (1-\theta)t_n$ takes the form:

$$\mathbf{C}_{n+\theta}\frac{\mathbf{T}_{n+1} - \mathbf{T}_n}{\Delta t} + \mathbf{K}_{n+\theta}\mathbf{T}_{n+\theta} = \mathbf{0}, \tag{8}$$

with $\mathbf{T}_{n+\theta} \equiv \mathbf{T}(t_{n+\theta}) = \theta\mathbf{T}_{n+1} + (1-\theta)\mathbf{T}_n$, $\mathbf{C}_{n+\theta} \equiv \mathbf{C}(\mathbf{T}_{n+\theta})$ and $\mathbf{K}_{n+\theta} \equiv \mathbf{K}(\mathbf{T}_{n+\theta})$.

By adopting the backward Euler scheme, which has 1st order accuracy and is unconditionally stable, $\theta = 1$ and it is obtained the following system:

$$\mathbf{C}_{n+1}\frac{\mathbf{T}_{n+1} - \mathbf{T}_n}{\Delta t} + \mathbf{K}_{n+1}\mathbf{T}_{n+1} = 0 \tag{9}$$

The above FEM formulation was implemented in MATLAB R2021a. To achieve reliable results, a mesh was optimized by dividing the unit cell into square elements (see Fig. 2 d–f). The x- and y-axis side were divided into 100 elements (10,000 squares generate the mesh), and it was adopted a time step of 600 s being the total time ($t_N$) 7.5 h. The optimization was carried out based on previous studies [19]. Finally, the computational time required to run the model is approximately 9 min on a laptop with 16 GB RAM and an Intel(R) Core(TM) i7-8565U processor.

## 4. Results

### 4.1. Mechanical properties

After 28 days of curing, compression strength tests were carried out on the three base systems (i.e., PC, SLAG and HSLAG mortars) with the different percentages of sand substitution by GW as it can be seen in Fig. 4. The results show that when the content of GW is increased, the bond between the binder and the aggregate is weaker, resulting in lower compressive strength values [58]. Moreover, as the GW is increased, the mixture needs a higher L/S ratio which introduces more porosity in the material, making it less resistant [59], as well as less conductive (Section 4.2).

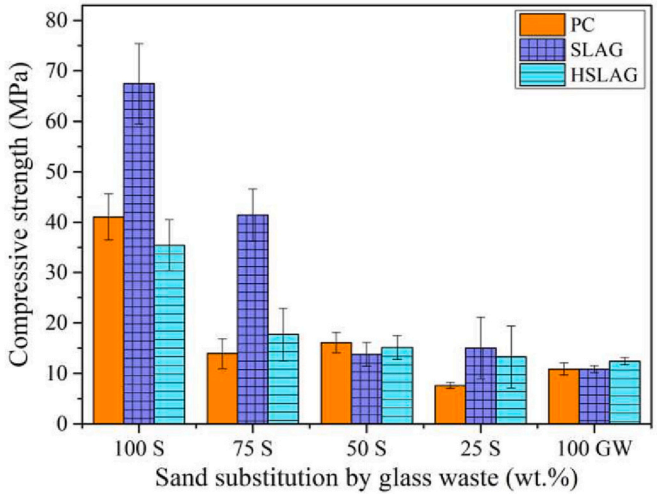


**Fig. 4.** Compressive strengths of the three different systems varying the sand substitution (wt.%) by GW. The vertical bars indicate the range between the minimum and the maximum value (among five repetition tests).

The best performance is achieved by the SLAG 100 S system (without sand substitution) which reaches a compressive strength value up to 67 MPa. This value, compared to the one obtained by the reference PC 100 S mortar, allows an improvement of 64%. This rise is due to the presence of silicon in the alkaline solution: a high cohesion and compaction of the main reaction product (C-A-S-H gel, because slag is used) is produced when the silicon is added using sodium silicate [37,60]. This enhanced behavior, as result of the highly amounts of cohesive gel, let the introduction of 25% by weight of GW replacing the sand in the AAM system (SLAG 75 S system). SLAG 75 S mortar obtains a compressive strength value of 41 MPa, which is equal to that obtained in the reference PC system without GW (namely, PC 100 S).

A reduction of only 13% is obtained if the HSLAG 100 S system is used instead of the PC 100 S mortar, as it obtains a value of 35 MPa. HSLAG 100 S mortar provides the lowest compressive strength due to its main reaction products, however, its value is comparable to that of the reference system. This result is given by its main reaction products that are mixtures of C-S-H gels (produced by the amount of PC of 17.5%) and C-A-S-H gel (produced by the 77.5 wt.% of slag in composition). The mixture of gels is not as consistency as the C-S-H gel present in the PC 100 S mortar. This is because in the reference sample a 100% of PC is used in contrast to the 17.5% employed in the HSLAG 100 S. Regarding the C-A-S-H gel, the one present in the hybrid system, is less cohesive than that of the AAM because no silica-rich solution is added.

Then, the four mortars which present the highest mechanical performance (i.e., PC 100 S, SLAG 100 S, SLAG 75 S, and HSLAG 100 S) were exposed to 20 thermal cycles between 200 °C and 400 °C to test their thermal stability for the use as TES. The mechanical behavior before (without treatment – WT) and after the exposure to thermal cycles is shown in Fig. 5.

It can be observed that the SLAG 100 S system keeps almost constant after thermal stress, decreasing its mechanical behavior by only 5%, thanks to the aforementioned C-A-S-H gel. The SLAG 75 S system shows the most drastic decline with a 25% reduction. The damage is produced due to the weak bond between aggregate and binder caused by incompatibility [61] and the continuous expansion of the aggregate during heating while the binder shrinks [62]. After the SLAG 75 S mortar, the reference PC 100 S mortar is the most affected by the thermal treatment, reducing its mechanical properties by 13%. The C-S-H produced in the reference sample is not as cohesive as the C-A-S-H gel of the SLAG 100 S, leading to a worse behavior against thermal cycles. Specifically, after 20 thermal cycles, SLAG 100 S has a compressive strength value 80% higher than PC 100 S. The HSLAG 100 S performance follows a trend contrary to that of other systems. The HM system improves its mechanical behavior by 6% after 20 cycles. This fact is produced because 28 days of curing is not enough time for the slag to precipitate/hydrate and form its main reaction products only in presence of water and a soft solid activator. Thus, when the mortar is heated, a reactivity in the HSLAG 100 S system is produced [44] leading to a 6% improvement in compressive strength compared to the PC 100 S sample after 20 cycles.

To understand the drop in the mechanical properties, porosity was also studied. Pores act like stress concentrators through which cracks tend to nucleate [63]. Cracks are produced due to shrinkage between the aggregate and the binder generated by the elevated temperature [64]. This phenomenon can be observed in Fig. 5, where an increase in porosity can be seen after thermal cycles and, consequently, the mechanical properties decrease. An exception is observed in the HSLAG 100 S, where the mechanical properties are influenced by the equilibrium between the reaction and the formation of the main hydration

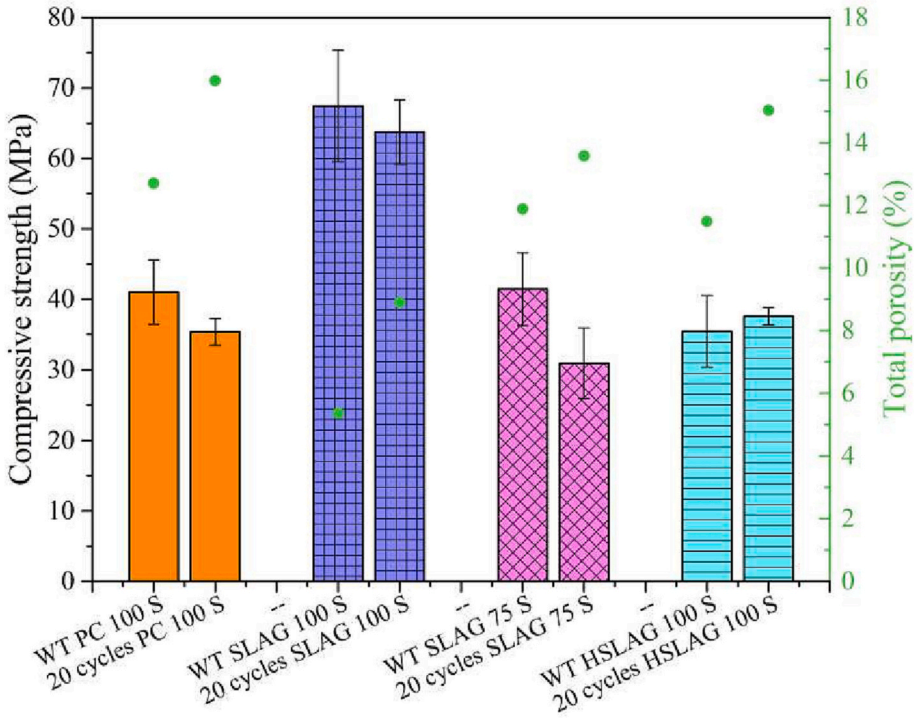


**Fig. 5.** Compressive strength and total porosity of selected systems before thermal treatment and after exposure to 20 thermal cycles. The vertical bars indicate the range between the minimum and the maximum value (among five repetition tests).

products (due to the application of heat) and the expansion/contraction of the aggregate/binder.

Porosity was calculated by using the difference between the theoretical and bulk densities values (Table 3). The theoretical densities increase or keep almost constant due to the shrinkage produced in the mortars after the thermal treatment.

### 4.2. Thermal properties

As shown in Fig. 6, after thermal treatments, a number of reactions and transformations take place which influence not only the mechanical properties but also the thermal properties, as the specific heat and thermal conductivity are affected [3].

Thermal conductivity is mainly affected by porosity. Pores hinder the propagation of phonons at atomistic scale, resulting in the interruption of heat transfer within the material [65,66]. But there are other properties that already affect this physical property such as the diameter of the particles, the bonding materials, the moisture content, the crystallinity of the material or the aging [67].

Before the thermal cycles, PC 100 S and SLAG 100 S samples show the highest thermal conductivity values (2.4 W/(m·K) and 2.5 W/(m·K), respectively). In the case of the SLAG 75 S mortar, due to the incompatibility between the binder and the aggregates, a reduction of 36% is obtained when compared to the reference PC sample. The thermal conductivity value of the HSLAG 100 S is 13% lower than that of the PC 100 S, this is due to its lower consistency of its main reaction products, already discussed in the previous section.

The thermal conductivity value of the SLAG 100 S system is 16% higher than that of the PC reference sample after exposure to 20 thermal cycles. In the case of the SLAG 75 S mortar, its thermal conductivity value is slightly lower (only 3% less) compared to the PC 100 S. Thermal conductivity values of the AAM systems are affected by 71% in the case of the SLAG 100 S and 60% in the case of the SLAG 75 S. The reference mortar is also affected by thermal stress, its value decrease compared to its untreated sample by 74%. The most affected thermal conductivity occurs in the HSLAG 100 S mortar, which obtains a reduction of 84% compared to the untreated sample. This again demonstrates the higher cohesiveness of the C-A-S-H gel compared to the C-S-H gel.

As with the mechanical behavior, the drop in thermal conductivity values is attributed to the porosity. The pores act as barriers to the propagation of phonons, thereby impacting heat transfer within the material. [19] After thermal cycles and exposure to high temperature, porosity increases in all systems due to expansion and contraction processes within the material. [64] Fig. 6 provides clearly evidence of the inverse relationship between porosity and thermal conductivity, where an increase of the porosity leads to a decrease in thermal conductivity.

The specific heat is the other important thermal property that must be consider, because, together with the mass of the material and the operational temperatures, it determines the amount of energy that can be stored in a block. Thermal cycles also strongly influence the maximum energy that can be stored in a material. This is due to the mass losses that occur during the heat treatment (i.e., evaporation of water, mass loss of the aggregates [14], decomposition of the gels and components [61,68–70], among others). The mass loss directly affects the specific heat. The most affected sample after 20 thermal cycles is the SLAG 75 S, which reduces its capacity from its untreated sample by 79% due to the aggregate expansion and the binder shrinkage [62] and due to the weak bond between the aggregate and the binder caused by incompatibility [61]. PC 100 S system follows the SLAG 75 S reducing its specific heat compared to its untreated sample by approximately 44%. Then, SLAG 100 S reduced its value by only 17% and HSLAG 100 S by about 29%.

**Table 3**
Theoretical (ρt) and bulk (ρb) densities.

| | WT | | 20 cycles | |
|---|---|---|---|---|
| | ρt (g/cm$^3$) | ρb (g/cm$^3$) | ρt (g/cm$^3$) | ρb (g/cm$^3$) |
| PC 100 S | 2.51 | 2.20 | 2.61 | 2.20 |
| SLAG 100 S | 2.43 | 2.30 | 2.42 | 2.21 |
| SLAG 75 S | 2.41 | 2.13 | 2.44 | 2.11 |
| HSLAG 100 S | 2.51 | 2.22 | 2.61 | 2.22 |

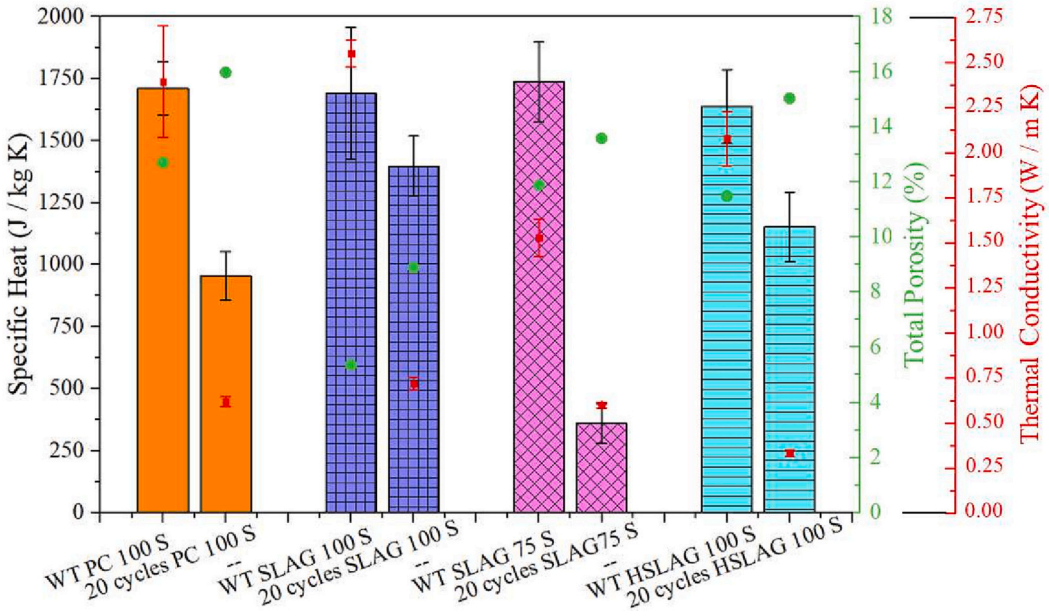


**Fig. 6.** Specific heat, thermal conductivity, and total porosity values of mortars without thermal treatment and after exposure to 20 thermal cycles. The vertical bars indicate the range between the minimum and the maximum value. For each property a different nu number of measurements were carried out, which are indicated in the experimental procedure.

It should be stress that, if the alternatives are compared to the PC 100 S system after the exposure to 20 cycles, there is an improvement in thermal storage capacity of >46% if the SLAG 100 S was used and almost 21% in the case of the HSLAG 100 S system. These major improvements coupled with the great impact of thermal cycles on the mechanical properties of the PC 100 S system, demonstrate again the possibility of using the alternative materials as TES in the CSP plants.

### 4.3. Finite element simulation

The parameters that were varied in the simulation were:

- Pipe arrangement: the most common configurations were analyzed. Triangular distribution with an angle of 30° and 45° between the center of the pipes, and square arrangement with an angle of 90°. These distributions can be seen in Fig. 2.
- Pipe diameter: two typical/standard outer diameters of an exchanger were chosen; 12.7 mm and 25.4 mm. To calculate the total surface of the tubes, a pipe thickness of 2 mm was considered.
- Number of pipes: the tubes were arranged in a 2-dimensional section of 3 × 3 $m^2$, where the distance between the centers (pitch) was varied. The section contains the maximum number of pipes according to the pitch.
- Pitch: the study was carried out for a pipe center distance of 70, 80, 90, 100, 100, 110, 110, 120, 130, 134, (based on a previous study to compare the results [14]), 140, 150, 150, 200, 300 and 400 mm.
- Material: bulk density, specific heat, and thermal conductivity of the four mortars that were exposed to 20 thermal cycles were included in the study to test the heat transfer phenomenon produced in the material. Those parameters are shown in Table 4.

To find a distribution that allows increasing operational temperatures (*Tmax* and *Tmin*) in Eq. (10) to improve the system efficiency by achieving higher sensible heat storage [23], the parameters mentioned before were varied. An increase in the thermal storage leads to a decrease in the number of blocks needed, which results in saving of costs, resources, and space. Thermal storage depends on the material of the block (as well as on the operational temperatures) as can be seen in Eq. (10), which is directly dependent on the specific heat. A high specific heat reduces the storage volume too. Construction materials commonly have a high specific heat but usually exhibit low thermal conductivities, therefore large heat exchanger surfaces are needed, as high thermal conductivity increases the dynamics in the system [13]:

**Table 4**
Thermal conductivity, specific heat and bulk density values required for the simulation.

| | Thermal conductivity, k, (W/(m × K)) after 20 thermal cycles | Specific heat, Cp, in the range of 290–390 °C (J/(kg × K)) after 20 thermal cycles | Bulk density, ρb, (g/cm$^3$) after 20 thermal cycles |
|---|---|---|---|
| PC 100 S | 0.62 | 953 | 2.20 |
| SLAG 100 S | 0.72 | 1397 | 2.21 |
| SLAG 75 S | 0.60 | 359 | 2.11 |
| HSLAG 100 S | 0.33 | 1152 | 2.22 |

$$Q = \int_{Tmin}^{Tmax} m\, Cp(T) dT \tag{10}$$

In order to know which arrangement provides the highest heating of the system in the shortest time, the same pitch (e.g., 100 mm) was chosen and simulations were carried out using the PC 100 S reference mortar after 20 thermal cycles to do the comparison among pipe distributions. Also, the diameter of the pipes was changed using the most common dimensions, 12.7 and 25.4 mm. Thus, the minimum unit cell colored in red in the 3 × 3 $m^2$ section was modelled as shown in Fig. 7.

After running the simulations, the fastest heating (as well as cooling) is obtained for the triangular distribution at an angle of 30° and with a diameter of 25.4 mm. This result was the expected because the contact area between tubes and block is larger and, consequently, there is less mass of mortar to be heated/cooled. With a 30° triangular distribution, the total number of tubes immersed in the section is 1003, i.e., 103 more tubes compared to the square distribution and 79 more tubes compared to the triangular distribution at an angle of 45°. Obviously, the surface area is also increased when the tube diameter rises. Thus, with a tube diameter of 25.4 mm, the TES is transferred faster from the tube to the

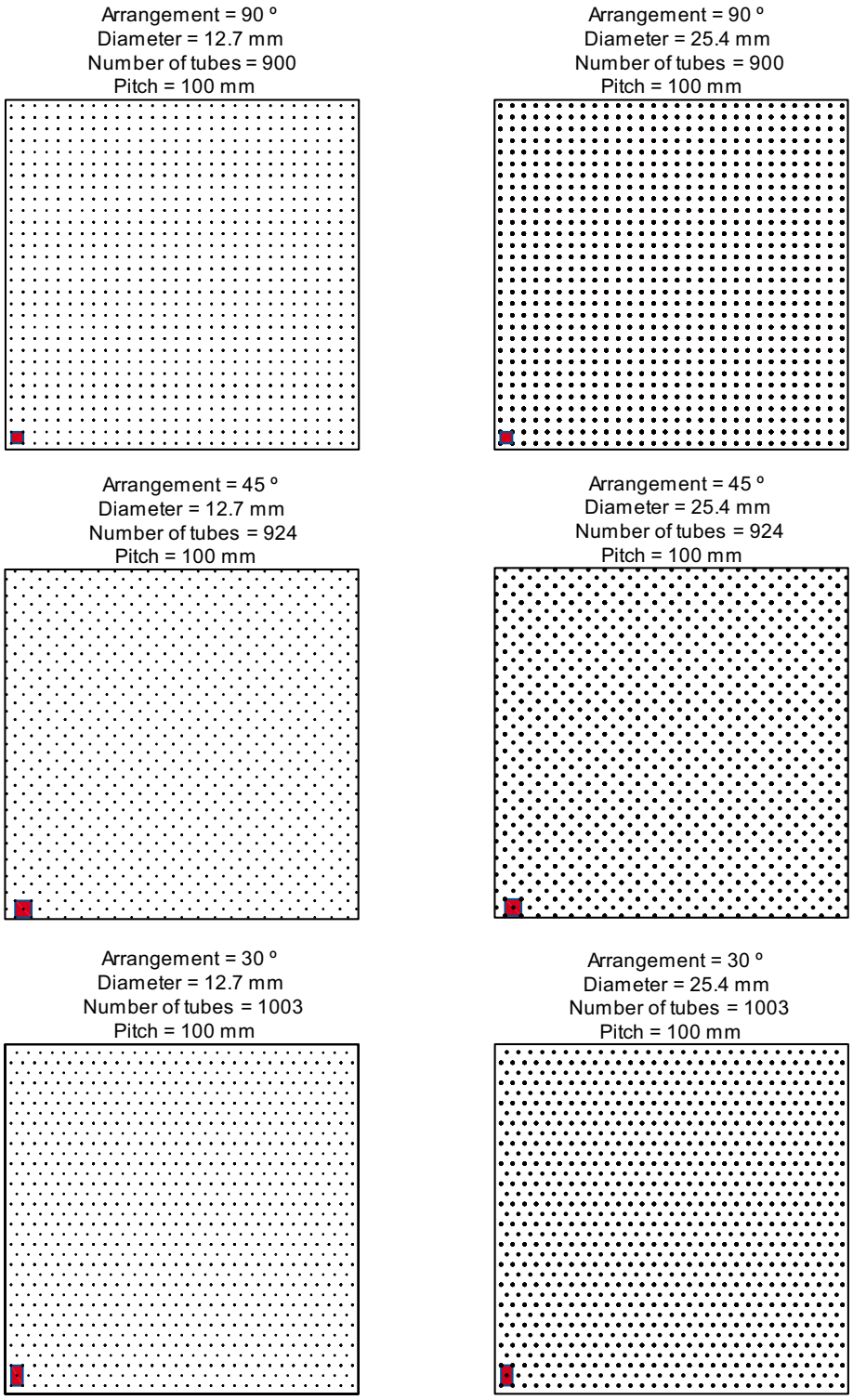


**Fig. 7.** Unit cells marked in red in the $3 \times 3$ m$^2$ sections for each of the chosen distributions. (For interpretation of the references to color in this figure legend, the reader is referred to the web version of this article.)

block (or vice versa in the discharge process of cooling) than with a tube diameter of 12.7 mm.

If we compare the systems with the same diameter (Fig. 8), let's say 25.4 mm, after 2 h of heating, if the square distribution with a 90° angle is used instead of the 30° triangular distribution, the heat transfer is reduced by 1.8%, while if the 45° triangular distribution is used, it is reduced by 1.6%. The heat transfer rate lies in the larger contact area of the triangular distribution with a 30° angle, because, if we look at Fig. 8, we can see that the number of tubes (NT) is higher for this tube configuration. This difference is greater after 2 h of charging if we compared the two different diameters using the same arrangement. For example, taking the 30° triangular distribution, the heat transfer is 4.4% faster if we use a diameter of 25.4 mm instead of 12.7 mm. This percentage decreases after a complete heating cycle, because after 7.5 h of storage, the temperature difference between the two systems is only 0.41%.

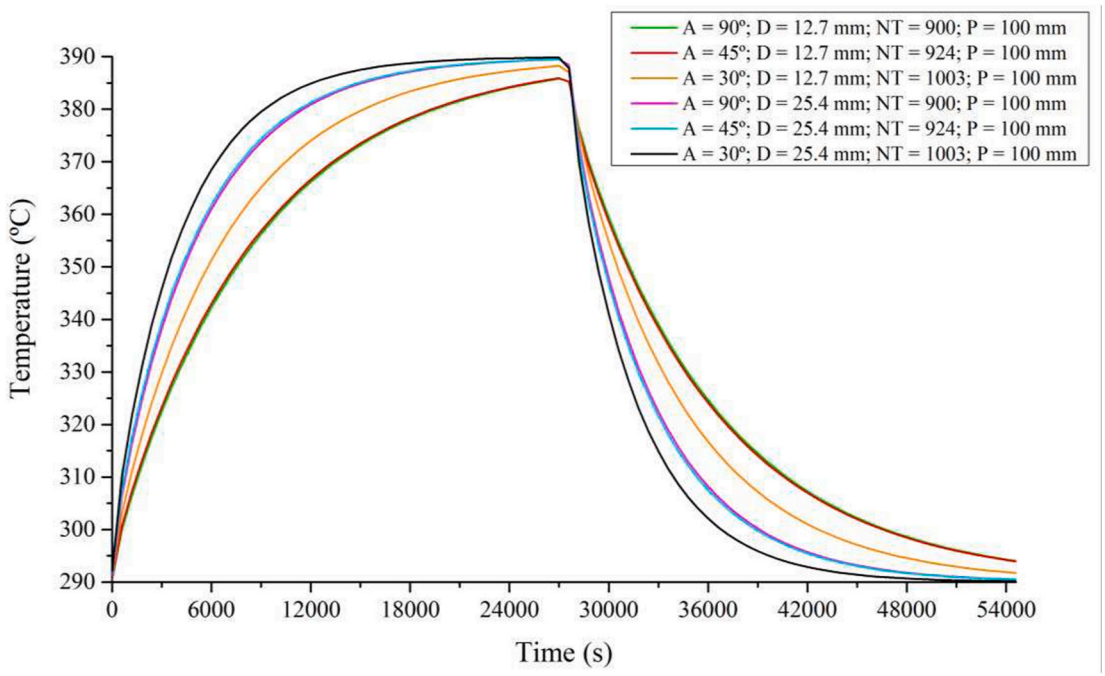


**Fig. 8.** Heating/cooling curves for different tube distributions with diameter variation. Pitch remains constant (100 mm).

Considering the higher temperature variation (leading to a greater stored energy as seen in Eq. (10)) reached by the 30° triangular system, and the small difference when the diameter was changed, the pitch was varied in the 30° triangular arrangement for both, the 12.7 mm and 25.4 mm diameters. The results for those geometries can be found in the Supplementary data section. The most optimal systems are chosen in order to make a discussion (systems highlighted in Tables 5, 6 and 7 of the Supplementary data section). Two restrictions were consider to choose the systems: for a load of 290 °C to 390 °C during 7.5 h of storage, the mortar must heat up to at least 380 °C (10 °C below the load temperature) and, in addition, its total volume to store at least 1100 MWh (meaning the capacity for a 50 MWel parabolic trough power plant of the ANDASOL-type [14]) is at most 30% higher than the current volume of the common Solar Salt (16,011 $m^3$ [71]). The systems which were selected can be seen for example in Fig. 9, where a comparison of the required volume to store 1100 MWh is made among the TES systems. Since a 30° triangular arrangement with a diameter of 25.4 mm results in a large heat exchanger surface area (element with the greatest economic impact), simulations were carried out keeping the 25.4 mm diameter, but choosing a square distribution to reduce the total number of tubes in the block.

- Volume of the TES systems

Fig. 9 shows the required volume of the selected systems to store at least 1100 MWh. None of the blocks made with SLAG 75 S mortar are

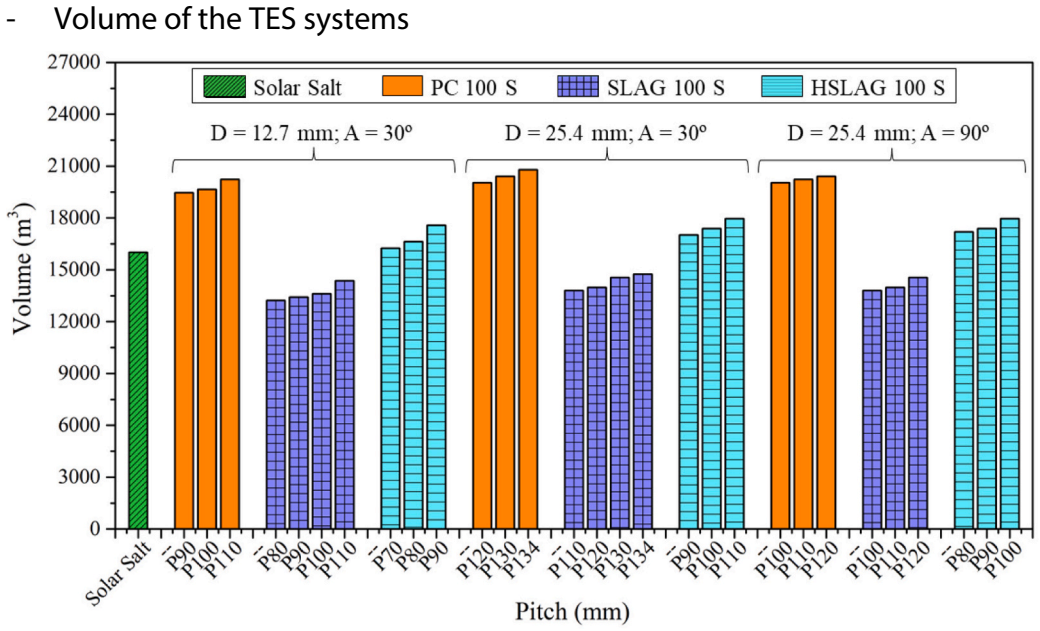


**Fig. 9.** Comparison of the volume required to store at least 1100 MWh ($m^3$).

taken into account because of its minimum volume required to store 1100 MWh for the three designs (a 30° triangular distribution with both diameters and a square distribution with a diameter of 25.4 mm) was >230% larger than the volume required for Solar Salt, which generates a high economic impact as it requires a large space for the installation of the TES in the CSP plant.

In contrast, the other alkali-activated system (SLAG 100 S) is the only one that, regardless the pitch, provides a volume decrease compared to Solar Salt. Specifically, when 30° triangular distribution, outer diameter of 12.7 mm and pitch of 80 mm are used in this material, 17% can be saved on the volume required for the TES installation. Even if the block design of the SLAG 100 S with a larger volume (30° triangular arrangement, 134 mm pitch and 25.4 mm diameter) was chosen, a volume saving of almost 8% could be achieved. If the minimum volume of the SLAG 100 S is compared to that of PC 100 S, 32% of space is saved. Even if the maximum volume of the SLAG 100 S system is compared to the minimum volume capable of being obtained by the PC 100 S, an improvement of >24% is obtained by the AAM mortar without GW.

In the case of the PC 100 S reference system, its minimum volume is obtained when combining a 30° triangular arrangement, diameter of 12.7 mm and a pitch of 90 mm, however, this system design requires almost 22% more volume than a TES system based on molten salts.

Although the use of HSLAG 100 S increases the volume, there is only an increase in volume compared to Solar Salt of >1% if the 30° triangular distribution with diameter 12.7 mm and pitch 70 mm is used. When comparing the minimum volume of this alternative mortar with the minimum volume of the reference sample (PC 100 S), there is an improvement of almost 17% when HSLAG 100 S is used. With this alternative, there is also an improvement of almost 8% if its block design with the highest volume is compared to the block of PC 100 S with the minimum volume.

- Total surface area of the heat exchanger

In addition to the TES volume, the total surface area of the heat exchanger must be considered due to the greatest economic impact of this element.

As Fig. 10 shows, while the pitch is increased in the same distribution, the total pipe surface decreases (fewer number of tubes in the block). For example, in a 30° triangular arrangement with a diameter of 12.7 mm, in the case of the reference sample, if the pitch increases from 90 mm to 110 mm, a saving of >30% is achieved. By varying the pitch, the greatest savings in the total pipe surface is obtained using a square distribution, with a diameter of 25.4 mm where the cementitious material is HSLAG 100 S. Specifically, there is a decrease if a pitch of 100 mm is used instead of 80 mm of almost 35%.

Another way to achieve large material savings is to reduce the diameter from 25.4 mm to 12.7 mm. This fact can be shown taking the same pitch (110 mm), the same material (such as SLAG 100 S) and the same pipe arrangement (30° triangular). The comparison shows that a reduction of >210% can be achieved. However, the most commonly used diameters in this application are not smaller than 20 mm [24,72].

It can be observed in Fig. 10 that there is only one block design that considers a total area under 100,000 $m^2$. This is the SLAG 100 S block, with triangular tube arrangement at an angle of 30°, with a pitch of 110 mm and a diameter of 12.7 mm. This result, compared to the PC 100 S system which has the smallest tube surface (D = 12,7 mm, Pitch = 110 mm, 30° triangular distribution), offers almost 29% material savings. Moreover, if the pitch was reduced to 100 mm in the SLAG 100 S, compared to the PC 100 S with the smaller tube surface, savings of almost 21% can be achieved. If the pitch of the AAM is further reduced to 90 mm, compared to the PC 100 S with minimum tube surface, a saving of almost 1% is obtained.

Considering the other alternative material, HSLAG 100 S system, the minimum tube surface is also achieved with a diameter of 12.7 mm but with a pitch of 90 mm. This option, compared to the PC 100 S with the minimum surface area, increases the total pipe surface (<30%). These results prove once again the feasibility of using alternative materials to PC as TES.

- Temperature increase/decrease

As it was mentioned before, the efficiency of TES is directly related to the operational temperatures (if the operational temperatures are increased, then, also the efficiency) [23]. The heat transfer rate is strictly linked to the material. Fig. 11 shows how the mortars increase/decrease their temperature during the charging/discharging process.

After a full charge cycle (7.5 h of warm-up), the difference between

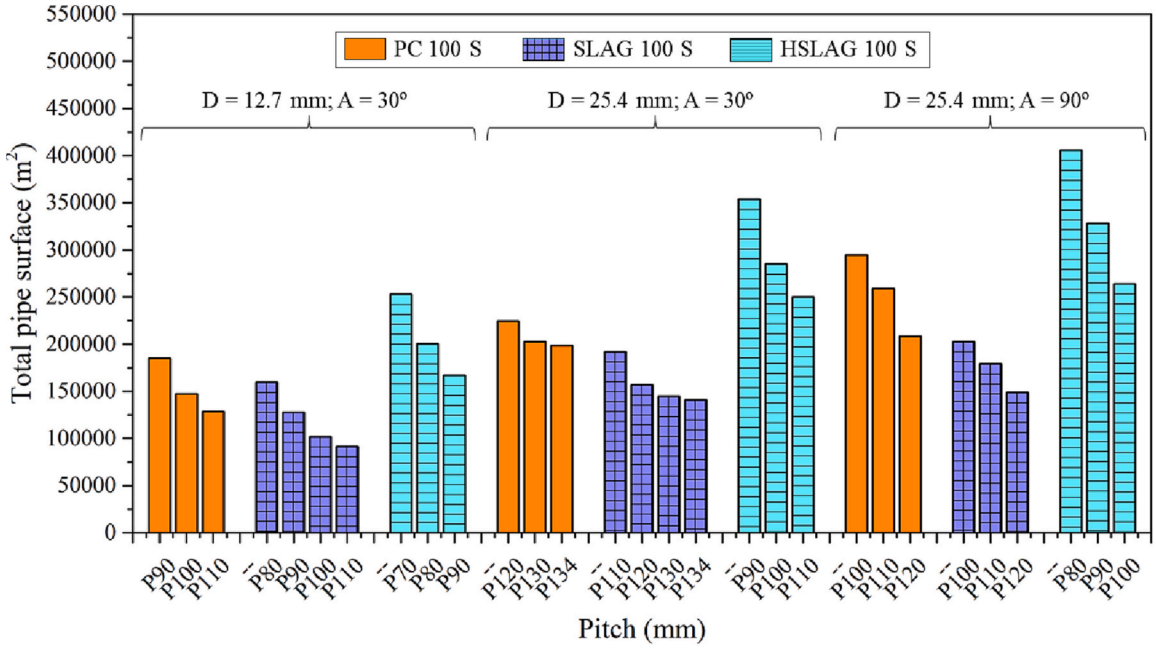


**Fig. 10.** Comparison of the total heat exchanger surface ($m^2$).

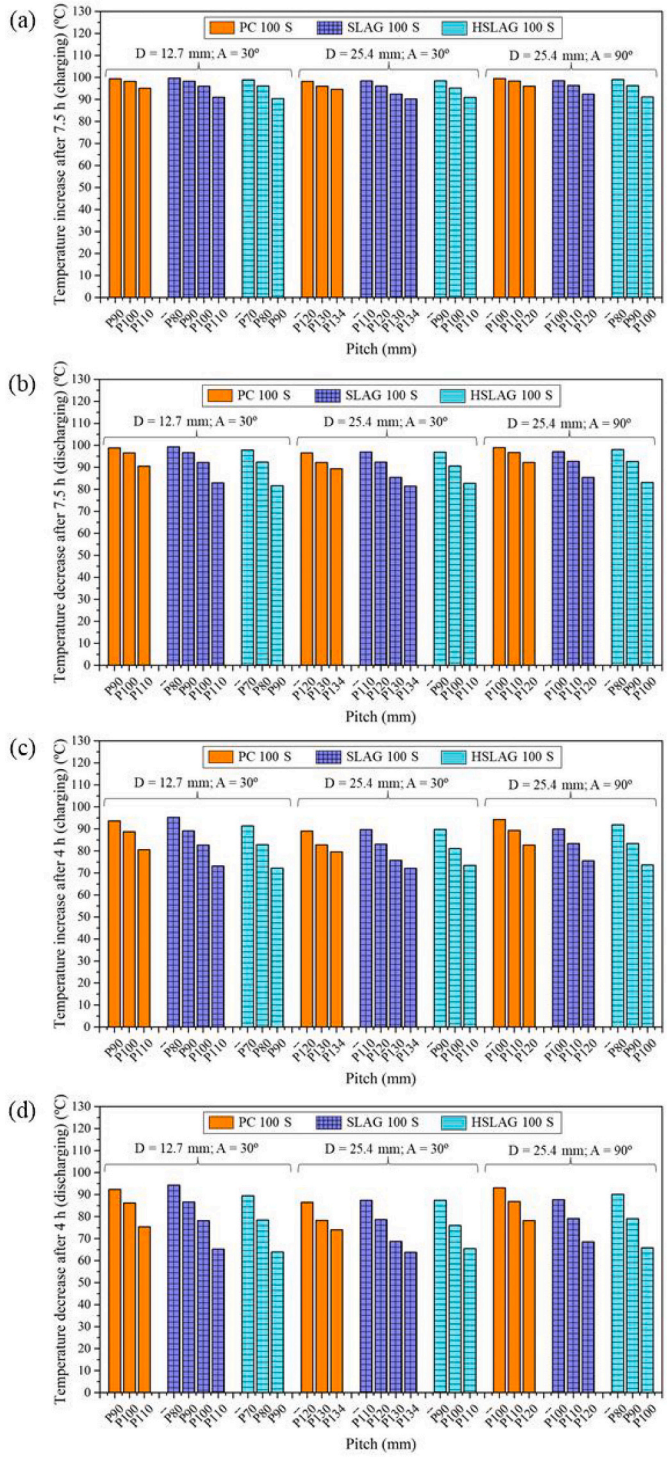


**Fig. 11.** Temperature increase/decrease (a) after 7.5 h of charging (b) after7.5 h of discharging (c) after 4 h of charging (d) after 4 h of discharging.

the temperature variations of each selected system is not too large (after that long period, a stationary point is almost reached in all systems). Specifically, the highest temperature variation is given by the SLAG 100 S with a diameter of 12.7 mm, a pitch of 80 mm and a 30° triangular pipe distribution (which increases its temperature by 99.65 °C) while the lowest temperature increase comes from the SLAG 100 S with a diameter of 25.4 mm, a pitch of 134 mm and a 30° triangular pipe distribution (it has an increment of 90.22 °C). So, there is only a difference of 9.42 °C between the system with the highest heat transfer rate and the system with the lowest one.

Although after a complete cycle of 7.5 h the temperature increase is very similar in all systems (see Fig. 11 (a)), it is worth mentioning that, although there is a 21% reduction of the total pipe surface (smaller contact area), as it has been already discussed above, if the SLAG 100 S with a 12.7 mm of diameter, a pitch of 100 mm and a 30° triangular distribution is chosen instead of the PC 100 S sample with the minimum heat exchanger surface (D = 12,7 mm, Pitch = 110 mm, 30° triangular distribution), the AAM system heats up after 7.5 h by about 1% more. Furthermore, reducing the pitch to 90 mm in the SLAG 100 S (D = 12,7 mm, 30° triangular distribution) results in a decrease in the total tube area compared to the PC 100 S with minimum tube surface of almost 1% and in a higher heating of the block (3% more) after 7.5 h. This demonstrates that not only an increase in the contact surface between the heat exchanger and the material provides a higher heating of the system also, the material of the TES is strongly related to the temperatures which can be reached. It exists a trade-off between the amount of energy stored and the efficiency of the charge process [28]. The better results of the SLAG 100 S system over the PC 100 S are because the AAM system counts with a higher thermal conductivity, so it increases the operating temperatures (higher heat transfer rate) and also, due to its high specific heat (>46% of the value of that of the PC 100 S), more energy can be stored in fewer blocks, which leads to material savings (cementitious materials and heat exchangers) and a reduction of the installation space. The performance of the SLAG 100 S as TES demonstrates what previous studies have confirmed, that a high heat capacity reduces the storage volume (less space needed) and a high thermal conductivity increases the dynamics in the system [13].

Considering the balance between operational temperatures and large investments caused by the tubes, if the HSLAG 100 S block which has the smallest contact surface (D = 12.7 mm, Pitch = 90 mm and a 30° triangular arrangement) is chosen, its temperature variation after the complete charging compared to the PC 100 S with the smallest surface is only 5% lower. This means that the HSLAG 100 S mortar also performs well and is comparable to the reference system.

Regarding the cooling process, it is important that the material keeps the heat inside for as many hours as possible to provide the HTF with heat when the source is not available. Also, it is important to have a slow and controlled cooling to avoid or minimize interfacial and external microcracks that may occur in the cementitious material [29]. Thus, in Fig. 11(b), the systems that present the better behavior are those which count with a lower temperature drop. It can be seen that the only systems with a decay lower than 85 °C are both alternative systems. Specifically, even though the SLAG 100 S with a diameter of 25.4 mm, a pitch of 134 mm and a 30° triangular pipe arrangement was the one that reaches the lowest temperature after the charging process (90.22 °C), it keeps its heat for a longer time resulting in a slower cooling of the block. So finally, after 7.5 h of cooling, it reduces its temperature from 380.22 °C (temperature reached after 7.5 h of heating) to 298.82 °C. This implies the lowest decay, just 81.40 °C. Following the previous system, the HSLAG 100 S block with a diameter of 12.7 mm, a pitch of 90 mm and a 30° triangular arrangement counts with a temperature drop of 81.65 °C. The lowest cooling by the reference sample (PC 100 S) occurs with a design diameter of 25.4 mm, a pitch of 134 mm and a 30° triangular arrangement. Its temperature drop is of 89.38 °C, which means that it cools down by >8% compared to the alternative mortars (provides less service when the source is not available).

After a complete charging/discharging cycle (7.5 h), a quasi-steady-state regime where the temperature does not change is reached. So, in order to have a better understanding of the behavior of the materials, the mortars were compared in the middle of the heating and cooling ramps (after 4 h) where the curve is steeper (this can be seen for example in Fig. 8). The variation of temperature and the stored energy after 4 h of charging/discharging process are shown in Tables 8/9 attached in the Supplementary data section.

Also, in Fig. 11(c), a comparison of the temperature variation after 4

h of heating can be seen. The design which heats up faster is the block made of SLAG 100 S with a diameter of 12.7 mm, a pitch of 80 mm and a 30° triangular distribution. It reaches a temperature increase of 95.24 °C. This design is followed by two blocks of the reference sample: the PC 100 S system with a diameter of 25.4 mm, a pitch of 100 mm and a square arrangement (that reaches a temperature increase of 94.25 °C) and the PC 100 S with a diameter of 12.7 mm, pitch of 90 mm and a 30° triangular arrangement (which increases its temperature by 93.66 °C). The main disadvantage of the reference sample is that, although it reaches very similar temperatures to the SLAG 100 S (D = 12.7 mm, Pitch = 80 mm, 30° triangular distribution), in the first case (D = 25.4 mm, Pitch = 100 mm, square arrangement) it has a larger heat exchanger surface, almost 85%, and in the second case (D = 12.7 mm, Pitch = 90 mm, 30° triangular distribution), it exceeds the pipe surface by >16%. This means that, in case the source is not available during a complete cycle (7.5 h), the SLAG 100 S system (D = 12.7 mm, Pitch = 80 mm, 30° triangular distribution) would store more energy given its higher heating rate, providing a cheaper solution than the one offered by PC 100 S due to the smaller heat exchanger surface required. After the mentioned systems, then, the HSLAG 100 S provides a temperature increment of 91.87 °C (using a diameter of 25.4 mm, a pitch of 80 mm and a square distribution) and 91.36 °C (using a diameter of 12.7 mm, a pitch of 70 mm and a 30° triangular distribution). This last configuration has a heat exchanger surface saving of >14% compared to the PC 100 S system which offers the higher heating rate.

As previously described, it is also important to consider slow cooling to keep the stored thermal energy longer (parameter discussed in the next point). In Fig. 11(d), after 4 h of discharging, the alternative systems show the lowest temperature decrease, as happened after 7.5 h of cooling. Specifically, SLAG 100 S (D = 25.4 mm, Pitch = 134 mm and a 30° triangular distribution) shows the smallest reduction (63.78 °C) followed by HSLAG 100 S (D = 12.7 mm, Pitch = 90 mm and a 30° triangular distribution) with a drop of 63.91 °C. Then, among the PC 100 S systems, the block design with a diameter pipe of 25.4 mm, pitch of 134 and 30° triangular arrangement, achieves a drop temperature of 73.98 (almost 14% more cooling than alternatives).

It has become clear that the important thing is to achieve a fast charging and a slow discharge, but always keeping the largest amount of stored energy.

- Stored energy

The number of blocks required for each system was calculated considering a storage of at least 1100 MWh (target stored energy). An integer number of blocks was set for each system as can be seen in Tables 5, 6 and 7. For this reason, it does not make sense to compare the maximum stored energy of mortars after 7.5 h, since the results are almost the same for all mortars. However, a good comparison for this

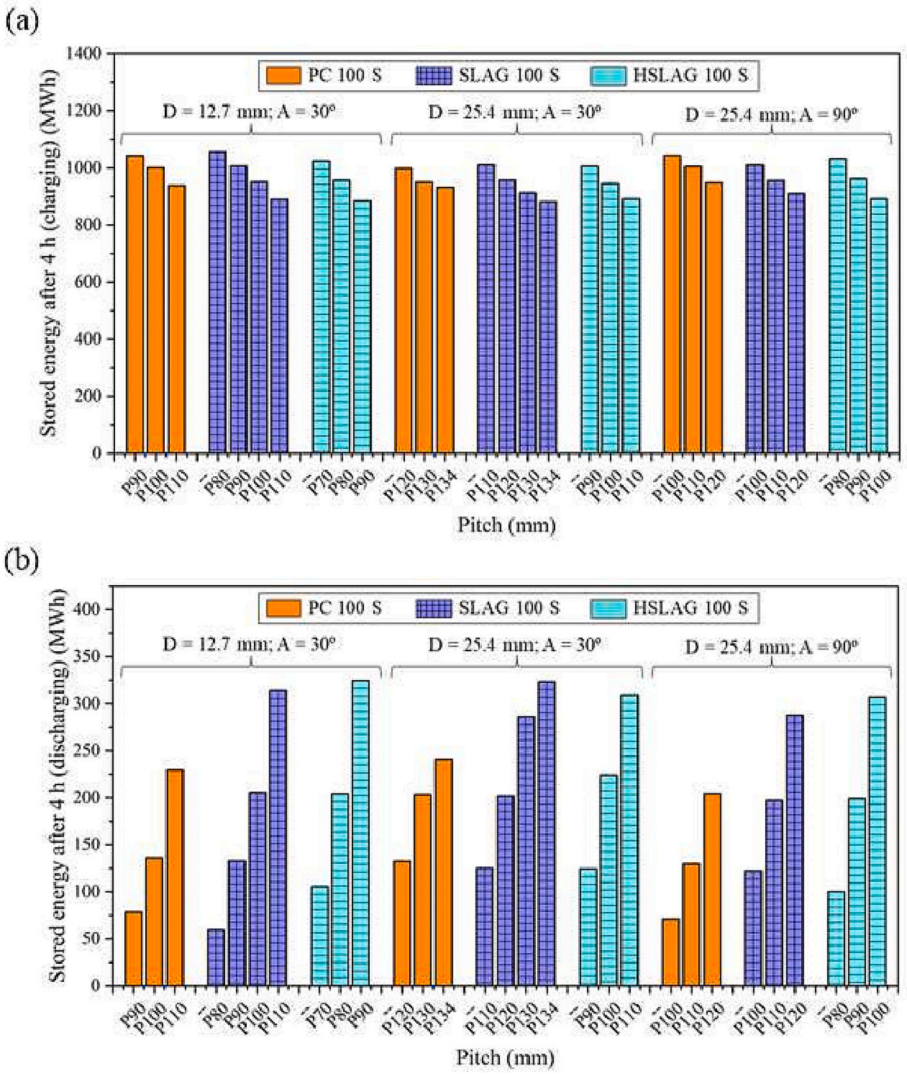


**Fig. 12.** Stored energy after 4 h of (a) charging (b) discharging.

parameter among all the systems can be made during the heating and cooling processes (after 4 h) because, as we have seen in the previous section, the temperature variations are not the same and this affects the stored energy as seen in Eq. (10). The stored energy comparison after 4 h can be observed in Fig. 12.

As it was expected, since the system with the highest thermal conductivity leads to the greatest temperature variation, as well as the system with the highest specific heat allows high TES, the SLAG 100 S with a diameter of 12.7 mm, a pitch of 80 mm and a 30° triangular distribution is able to store more energy than the rest. Specifically, after 4 h, it harvests 1056 MWh. Then, the PC 100 S system with a diameter of 25.4 mm, a pitch of 100 mm and a square arrangement stores 1044 MWh and the PC 100 S with a diameter of 12.7 mm, pitch of 90 mm and a 30° triangular arrangement, 1043 MWh. The difference between the reference system and the SLAG 100 S (D = 12.7 mm, Pitch = 80 mm and a 30° triangular distribution) is the number of blocks needed to store at least 1100 MWh: 36 more in the first case (D = 25.4 mm, Pitch = 100 mm and square arrangement) and 33 more in the second (D = 12.7 mm, Pitch = 90 mm and a 30° triangular distribution). More in detail, after 4 h, the first mentioned PC 100 S system needs 46% more mass than the SLAG 100 S (D = 12.7 mm, Pitch = 80 mm, 30° triangular arrangement) to store 1044 MWh (12 MWh less) while, the second system requires a 47% more mass compared to the alternative to store 1043 MWh (13 MWh less).

Then, the results for the HSLAG 100 S mortars are lower but fully comparable and useful for the application. HSLAG 100 S with diameter of 25.4 mm, a pitch of 80 mm and square distribution stores 1031 MWh and HSLAG 100 S with diameter of 12.7 mm, a pitch of 70 mm and 30° triangular distribution stores 1024 MWh. The PC 100 S system that stores more energy (1044 MWh after 4 h) needed less mortar (mass) compared to the PC 100 S with a diameter of 12.7 mm, pitch of 90 mm and a 30° triangular arrangement, but still needs slightly >16% mass compared to the HSLAG 100 S systems.

Focusing on the stored TES after 4 h of discharge, the results show that, although the SLAG 100 S with 25.4 mm diameter, 134 mm pitch and 30° triangular distribution shows the lowest temperature decay, it is not the mortar that maintains the highest energy after 4 h of cooling. The system that maintains the highest energy (324 MWh) is the HSLAG 100 S with 12.7 mm diameter and 90 mm pitch. This is because it loses its heat very slow due to its low thermal conductivity. Next, with 323 MWh and 314 MWh, two SLAG 100 S systems succeed the previous HSLAG 100 S: the one described above (D = 25.4 mm, Pitch = 134 mm and 30° triangular distribution) and the system with a diameter of 12.7 mm, pitch of 110 mm and triangular distribution with a 30° angle, respectively.

It is important to highlight that the performance of the SLAG 100 S block (D = 12.7 mm, Pitch = 110 mm and 30° triangular distribution) because it proves once again its great advantages for a CSP plant. Among all the systems, it has the smallest heat exchanger surface area (it is the cheapest as it does not require as many tubes), it is one of the mortars which maintains the energy for a longer period, its maximum temperature reached after a complete cycle is not even 9% below the fastest heating system (SLAG 100 S with a diameter of 12.7 mm, pitch of 80 mm and triangular distribution with an angle of 30°) and it provides a reduction of >10% compared to the typical Solar Salt.

Concerning the reference sample, after 4 h of discharging (when the cycle has 3.5 h left to run), none of the designed block manages to maintain an energy of 300 MWh. The PC 100 S mortar which maintains energy better is that with a diameter of 25.4 mm, a pitch of 134 mm and a 30° distribution stores, after 4 h of cooling, reaches 241 MWh: at this point of the cycle has less energy than the alternatives mentioned (>23%).

As final comment, it can be stated that all the parameters obtained from the Finite Element Simulation indicate that the alternative mortars are very good options to work as TES systems in CSP plants. In fact, different designs show an improvement over the reference PC 100 S material.

## 5. Conclusions

After the experimental and the computational studies, it can be stated that:

- The high cohesion of the C-A-S-H gel provides better mechanical properties to the alkali-activates systems. SLAG 100 S system keeps almost constant its strength after the exposure to 20 thermal cycles, between 200 °C and 400 °C, providing an 80% higher resistance compared to the reference PC 100 S system. In the case of the SLAG 75 S system, without any thermal treatment, it achieves the same resistance as the PC 100 S. However, after 20 cycles, the compressive strength of the SLAG 75 S decreases by 12% compared to the PC 100 S.
- The damage of the HSLAG 100 S system, under treatments of thermal cycles, is not as big as in the other systems, specifically, when it is exposed to the thermal treatment it outperforms the PC 100 S in 6%.
- Porosity influences both mechanical and thermal properties because air cavities cause a detriment in both aspects. For this reason, porosity is a property that must be considered if a material is going to be used as TES medium. Lower porosity improves the use of cementitious materials as TES. The SLAG 100 S system has the lowest porosity values before and after thermal cycling.
- The exposure of a material to thermal cycles also affects thermal properties. The alternatives offer similar thermal conductivities to PC 100 S. In particular, the SLAG 100 S system, operating in cycles as it would do it in CSP technology, improves the thermal conductivity after exposure by 16% compared to PC. In the case of the specific heat, the high values (measured via DSC tests) of the SLAG 100 S and HSLAG 100 S after 20 thermal cycles allow an increase in stored energy compared to the reference mortar. Energy storage capacity is improved over that of the PC 100 S by >46%, using the SLAG 100 S, and by around 21% for the HSLAG 100 S.
- FEM simulations allowed to describe which typical geometry increased the temperature variation in order to achieve higher efficiency in the TES system. The highest temperature rise (after 2 h of heating increases heat transfer by >1.6% compared to the other two configurations) is achieved with a system that arranges the tubes in a triangular distribution with an angle of 30°.
- The only mortar capable of reducing the volume of the typical Solar Salt, while storing the same energy (1100 MWh), is the SLAG 100 S. Volume savings of 17% can be achieved. Comparing this alternative with the reference sample, a decrease in volume of 32% can be obtained. The volume of the other alternative, HSLAG system, is comparable to that of molten salt, with the right design, only 1% more can be achieved compared to the Solar Salt. Comparing the minimum volume of the HSLAG 100 S mortar with the minimum volume of the PC 100 S system, there is an improvement of almost 17% when the alternative is used.
- The main way to save the cost in a TES system is to reduce the contact surface of the heat exchangers. This can be achieved by reducing the diameter of the pipes, increasing the pitch, or using materials with high specific heat (to store more energy) and high thermal conductivity (to increase the dynamics of the CSP plants). Thus, the SLAG 100 S mortar is the most efficient system, reducing the total pipe surface by up to 29% compared to the reference material.
- To choose the most optimal TES system is important to consider: an optimal heat transfer rate, a small volume of the system to save space and the smallest pipe surface to minimize economic impact. Considering all these parameters, the SLAG 100 S system with a diameter of 12.7 mm, pitch of 110 mm and triangular distribution with a 30° angle seems to be the most suitable for the application.

Although PC is currently proving to be a promising material to use it

as TES, this study has found that its alternative materials, hybrid and alkali-activated materials, can offer greater efficiency for operation in CSP plants, as they provide better mechanical and thermal performance. Therefore, alternative materials to PC systems can be considered for use as TES media opening new gates towards use of renewable energies.

## CRediT authorship contribution statement

**Irene Ramón-Álvarez:** Conceptualization, Investigation, Methodology, Resources, Formal analysis, Data curation, Writing – original draft. **Sergio Sánchez-Delgado:** Conceptualization, Writing – review & editing, Validation, Supervision, Funding acquisition. **Ignacio Peralta:** Software, Supervision, Conceptualization, Writing – review & editing, Validation. **Antonio Caggiano:** Software, Supervision, Conceptualization, Writing – review & editing, Validation. **Manuel Torres-Carrasco:** Conceptualization, Resources, Writing – original draft, Validation, Supervision, Funding acquisition, Writing – review & editing.

## Declaration of competing interest

The authors declare that they have no known competing financial interests or personal relationships that could have appeared to influence the work reported in this paper.

## Data availability

Data will be made available on request.

## Acknowledgment

This study was funded by MCIN/AEI/10.13039/501100011033 and Europe Union NextGenerationEU/PRTR under the National Project TED2021-130633B-I00 and under the National Project PID2021-125810OB-C22. In addition, we would like to thank the Álvaro Alonso Barba Institute (IAAB-UC3M) for granting a pre-doctoral grant for a stay at the University of Genoa.

## Appendix A. Supplementary data

Supplementary data to this article can be found online at https://doi.org/10.1016/j.est.2023.108076.

## References

[1] UNFCC, COP26 Explained, 2021.
[2] S. Zhang, W. Chen, Assessing the energy transition in China towards carbon neutrality with a probabilistic framework, Nat. Commun. 13 (2022), https://doi.org/10.1038/s41467-021-27671-0.
[3] A. Gil, M. Medrano, I. Martorell, A. Lázaro, P. Dolado, B. Zalba, L.F. Cabeza, State of the art on high temperature thermal energy storage for power generation. Part 1-concepts, materials and modellization, Renew. Sust. Energ. Rev. (2010), https://doi.org/10.1016/j.rser.2009.07.035.
[4] G. Alva, Y. Lin, G. Fang, An Overview of Thermal Energy Storage Systems, Energy, 2018, https://doi.org/10.1016/j.energy.2017.12.037.
[5] H. Zhang, J. Baeyens, G. Cáceres, J. Degrève, Y. Lv, Thermal energy storage: recent developments and practical aspects, Prog. Energy Combust. Sci. (2016), https://doi.org/10.1016/j.pecs.2015.10.003.
[6] M. Haider, A. Werner, An overview of state of the art and research in the fields of sensible, latent and thermo-chemical thermal energy storage, Elektrotechnik Und Informationstechnik (2013), https://doi.org/10.1007/s00502-013-0151-3.
[7] L. Boquera, J.R. Castro, A.L. Pisello, C. Fabiani, A. D'Alessandro, F. Ubertini, L. F. Cabeza, Thermal and mechanical performance of cement paste under high temperature thermal cycles, Sol. Energy Mater. Sol. Cells (2021), https://doi.org/10.1016/j.solmat.2021.111333.
[8] R. Tamme, D. Laing, W.D. Steinmann, Advanced thermal energy storage technology for parabolic trough, in: Int. Sol. Energy Conf, 2003, https://doi.org/10.1115/ISEC2003-44033.
[9] F. Aarab, B. Kuhn, A. Bonk, T. Bauer, A new approach to low-cost, solar salt-resistant structural materials for concentrating solar power (CSP) and thermal energy storage (TES) _ Enhanced Reader.pdf, Metals (Basel) 11 (2021) 1970, https://doi.org/10.3390/met11121970.
[10] R. Li, H. Zhang, H. Wang, Q. Tu, X. Wang, Integrated hybrid life cycle assessment and contribution analysis for CO2 emission and energy consumption of a concentrated solar power plant in China, Energy (2019), https://doi.org/10.1016/j.energy.2019.02.066.
[11] U. Herrmann, D.W. Kearney, Survey of thermal energy storage for parabolic trough power plants, J. Sol. Energy Eng. Trans. ASME (2002), https://doi.org/10.1115/1.1467601.
[12] D. Brosseau, J.W. Kelton, D. Ray, M. Edgar, K. Chisman, B. Emms, Testing of thermocline filler materials and molten-salt heat transfer fluids for thermal energy storage systems in parabolic trough power plants, J. Sol. Energy Eng. Trans. ASME (2005), https://doi.org/10.1115/1.1824107.
[13] D. Laing, W.D. Steinmann, M. Fiß, R. Tamme, T. Brand, C. Bahl, Solid media thermal storage development and analysis of modular storage operation concepts for parabolic trough power plants, in: J. Sol. Energy Eng. Trans. ASME, 2008, https://doi.org/10.1115/1.2804625.
[14] D. Laing, C. Bahl, T. Bauer, M. Fiss, N. Breidenbach, M. Hempel, High-temperature solid-media thermal energy storage for solar thermal power plants, in: Proc. IEEE, 2012, https://doi.org/10.1109/JPROC.2011.2154290.
[15] D. Laing, W.D. Steinmann, R. Tamme, C. Richter, Solid media thermal storage for parabolic trough power plants, Sol. Energy (2006), https://doi.org/10.1016/j.solener.2006.06.003.
[16] N. Hoivik, C. Greiner, E.B. Tirado, J. Barragan, P. Bergan, G. Skeie, P. Blanco, N. Calvet, Demonstration of EnergyNest thermal energy storage (TES) technology, in: AIP Conf. Proc, 2017, https://doi.org/10.1063/1.4984432.
[17] M. Martins, U. Villalobos, T. Delclos, P. Armstrong, P.G. Bergan, N. Calvet, New concentrating solar power facility for testing high temperature concrete thermal energy storage, in: Energy Procedia, 2015, https://doi.org/10.1016/j.egypro.2015.07.350.
[18] P.G. Bergan, C.J. Greiner, A new type of large scale thermal energy storage, in: Energy Procedia, 2014, https://doi.org/10.1016/j.egypro.2014.10.422.
[19] I. Ramón-Álvarez, C. Marugán-Cruz, E. Enríquez, S. Sánchez-Delgado, M. Torres-Carrasco, Alkali-activated and hybrid materials: alternative to Portland cement as a storage media for solar thermal energy, in: Boletín La Soc. Española Cerámica y Vidr, 2021, https://doi.org/10.1016/j.bsecv.2021.11.006.
[20] Y.C. Hua, T. Zhao, Z.Y. Guo, Transient thermal conduction optimization for solid sensible heat thermal energy storage modules by the Monte Carlo method, Energy (2017), https://doi.org/10.1016/j.energy.2017.05.073.
[21] C.R.C. Rao, H. Niyas, P. Muthukumar, Performance tests on lab–scale sensible heat storage prototypes, Appl. Therm. Eng. (2018), https://doi.org/10.1016/j.applthermaleng.2017.10.085.
[22] F. Bai, C. Xu, Performance analysis of a two-stage thermal energy storage system using concrete and steam accumulator, Appl. Therm. Eng. (2011), https://doi.org/10.1016/j.applthermaleng.2011.04.049.
[23] R.P. Selvam, M. Castro, 3D FEM model to improve the heat transfer in concrete for thermal energy storage in solar power generation, in: ASME 2010 4th Int. Conf. Energy Sustain. ES 2010, 2010, https://doi.org/10.1115/ES2010-90078.
[24] C. Ferone, F. Colangelo, D. Frattini, G. Roviello, R. Cioffi, R. di Maggio, Finite element method modeling of sensible heat thermal energy storage with innovative concretes and comparative analysis with literature benchmarks, Energies (2014), https://doi.org/10.3390/en7085291.
[25] M.D. Muhammed, O. Badr, Analysis of a hybrid cascaded latent/sensible storage system for parabolic-trough solar thermal plants, J. Therm. Eng. (2021), https://doi.org/10.18186/THERMAL.888469.
[26] H. Shabgard, T.L. Bergman, N. Sharifi, A. Faghri, High temperature latent heat thermal energy storage using heat pipes, Int. J. Heat Mass Transf. (2010), https://doi.org/10.1016/j.ijheatmasstransfer.2010.03.035.
[27] K. Nithyanandam, R. Pitchumani, Analysis and optimization of a latent thermal energy storage system with embedded heat pipes, Int. J. Heat Mass Transf. (2011), https://doi.org/10.1016/j.ijheatmasstransfer.2011.06.018.
[28] K. Bataineh, A. Gharaibeh, Optimal design for sensible thermal energy storage tank using natural solid materials for a parabolic trough power plant, Sol. Energy (2018), https://doi.org/10.1016/j.solener.2018.06.108.
[29] G.M. Giannuzzi, R. Liberatore, D. Mele, G. Mazzucco, G. Xotta, V.A. Salomoni, C. E. Majorana, R. Di Maggio, Experimental campaign and numerical analyses of thermal storage concrete modules, Sol. Energy (2017), https://doi.org/10.1016/j.solener.2017.08.041.
[30] E. Özrahat, S. Ünalan, Thermal performance of a concrete column as a sensible thermal energy storage medium and a heater, Renew. Energy (2017), https://doi.org/10.1016/j.renene.2017.04.046.
[31] U. Herrmann, B. Kelly, H. Price, Two-tank molten salt storage for parabolic trough solar power plants, Energy (2004), https://doi.org/10.1016/S0360-5442(03)00193-2.
[32] R. Kumar, A.K. Pathak, M. Kumar, A.K. Patil, Experimental study of multi tubular sensible heat storage system fitted with wire coil inserts, Renew. Energy (2021), https://doi.org/10.1016/j.renene.2020.10.058.
[33] N. Shehata, E.T. Sayed, M.A. Abdelkareem, Recent progress in environmentally friendly geopolymers: a review, Sci. Total Environ. (2021), https://doi.org/10.1016/j.scitotenv.2020.143166.
[34] E. Benhelal, G. Zahedi, E. Shamsaei, A. Bahadori, Global strategies and potentials to curb CO2 emissions in cement industry, J. Clean. Prod. 51 (2013) 142–161, https://doi.org/10.1016/j.jclepro.2012.10.049.
[35] R. Feiz, J. Ammenberg, M. Eklund, A. Helgstrand, R. Marshall, Improving the CO2 performance of cement, part I: utilizing life-cycle assessment and key performance indicators to assess development within the cement industry, J. Clean. Prod. 98 (2015) 272–281, https://doi.org/10.1016/J.JCLEPRO.2014.01.083.

[36] E. Batuecas, I. Ramón-Álvarez, S. Sánchez-Delgado, M. Torres-Carrasco, Carbon footprint and water use of alkali-activated and hybrid cement mortars, J. Clean. Prod. (2021), https://doi.org/10.1016/j.jclepro.2021.128653.
[37] F. Puertas, M. Torres-Carrasco, Use of glass waste as an activator in the preparation of alkali-activated slag. Mechanical strength and paste characterisation, Cem. Concr. Res. 57 (2014) 95–104, https://doi.org/10.1016/j.cemconres.2013.12.005.
[38] M. Torres-Carrasco, J.G. Palomo, F. Puertas, Sodium silicate solutions from dissolution of glass wastes: statistical analysis, Mater. Constr. 64 (2014), https://doi.org/10.3989/mc.201405213.
[39] I. Garcia-Lodeiro, N. Boudissa, A. Fernandez-Jimenez, A. Palomo, Use of clays in alkaline hybrid cement preparation. The role of bentonites, Mater. Lett. 233 (2018) 134–137, https://doi.org/10.1016/j.matlet.2018.08.098.
[40] I. Amer, M. Kohail, M.S. El-Feky, A. Rashad, M.A. Khalaf, Characterization of alkali-activated hybrid slag/cement concrete, Ain Shams Eng. J. (2021), https://doi.org/10.1016/j.asej.2020.08.003.
[41] P. Duxson, J.L. Provis, G.C. Lukey, J.S.J. van Deventer, The role of inorganic polymer technology in the development of 'green concrete', Cem. Concr. Res. 37 (2007) 1590–1597.
[42] C. Shi, B. Qu, J.L. Provis, G. Habert, J.B. D'Espinose De Lacaillerie, N. Roussel, Recent progress in low-carbon binders, J. Clean. Prod. 122 (2019) 227–250, https://doi.org/10.1016/j.cemconres.2019.05.009.
[43] G. Habert, J.B. d'Espinose de Lacaillerie, N. Roussel, An environmental evaluation of geopolymer based concrete production: reviewing current research trends, J. Clean. Prod. 19 (2011) 1229–1238, https://doi.org/10.1016/j.jclepro.2011.03.012.
[44] I. Garcia-Lodeiro, A. Fernandez-Jimenez, A. Palomo, Hydration kinetics in hybrid binders: Early reaction stages, Cement and Concrete Composites 39 (2013) 82–92. ISO 690.
[45] N.B.R. Monteiro, J.M. Moita Neto, E.A. da Silva, Environmental assessment in concrete industries, J. Clean. Prod. (2021), https://doi.org/10.1016/j.jclepro.2021.129516.
[46] G.K. Chaturvedy, U.K. Pandey, Performance characteristics of rubberized concrete: a multipoint review, Innov. Infrastruct. Solut. (2022), https://doi.org/10.1007/s41062-021-00637-3.
[47] UNE-EN 196-1, UNE-EN 196-1 Métodos de ensayo de cementos - parte 1: determinación de resistencias mecánicas, Eur. Stand. (2005).
[48] A. Fernández-Jiménez, I. Garcia-Lodeiro, O. Maltseva, A. Palomo, Hydration mechanisms of hybrid cements as a function of the way of addition of chemicals, J. Am. Ceram. Soc. (2019), https://doi.org/10.1111/jace.15939.
[49] S. Shagñay, L. Ramón, M. Fernández-álvarez, A. Bautista, F. Velasco, M. Torres-Carrasco, Eco-efficient hybrid cements: pozzolanic, mechanical and abrasion properties, Appl. Sci. 10 (2020) 1–15, https://doi.org/10.3390/app10248986.
[50] AENOR, UNE-EN 196-3:2017. Métodos de ensayo de cementos. Parte 3: Determinación del tiempo de fraguado y de la estabilidad de volumen, 2017, pp. 3–6.
[51] T. Lucio-Martin, J. Puentes, M.C. Alonso, Effect of geometry in concrete spalling risk subjected to high temperatures for thermal inertia studies, in: Proc. From 6th Int. Work. Concr. Spalling vol. 1, 2019, pp. 71–80.
[52] N. Algourdin, P. Pliya, A.L. Beaucour, A. Simon, A. Noumowé, Influence of polypropylene and steel fibres on thermal spalling and physical-mechanical properties of concrete under different heating rates, Constr. Build. Mater. (2020), https://doi.org/10.1016/j.conbuildmat.2020.119690.
[53] M. Roig-Flores, T. Lucio-Martin, M.C. Alonso, L. Guerreiro, Evolution of thermo-mechanical properties of concrete with calcium aluminate cement and special aggregates for energy storage, Cem. Concr. Res. (2021), https://doi.org/10.1016/j.cemconres.2020.106323.
[54] AENOR, UNE-EN 993-1:2018 (Ratificada) Métodos de ensayo para productos refractarios conformados densos. Parte 1: Determinación de la densidad aparente, de la porosidad abierta y de la porosidad total. (Ratificada por la Asociación Española de Normalización en en), 2019.
[55] J. Saari, Heat Exchanger Dimensioning, 2011, pp. 1–101. https://sistemas.eel.usp.br/docentes/arquivos/5817712/LOQ4086/saari_heat_exchanger_dimensioning.pdf.
[56] I. Peralta, V.D. Fachinotti, E.A.B. Koenders, A. Caggiano, Computational design of a massive solar-thermal collector enhanced with phase change materials, Energy Build. (2022), https://doi.org/10.1016/j.enbuild.2022.112437.
[57] O.C. Zienkiewicz, R.L. Taylor, The Finite Element Method. Volume 1: Basic Formulation and Linear Problems, 1994.
[58] T.C. Ling, C.S. Poon, H.W. Wong, Management and recycling of waste glass in concrete products: current situations in Hong Kong, Resour. Conserv. Recycl. (2013), https://doi.org/10.1016/j.resconrec.2012.10.006.
[59] S. De Castro, J. De Brito, Evaluation of the durability of concrete made with crushed glass aggregates, J. Clean. Prod. (2013), https://doi.org/10.1016/j.jclepro.2012.09.021.
[60] M. Torres-Carrasco, F. Puertas, Waste glass as a precursor in alkaline activation: chemical process and hydration products, Constr. Build. Mater. 139 (2017) 342–354, https://doi.org/10.1016/j.conbuildmat.2017.02.071.
[61] F. Kantarci, İ. Türkmen, E. Ekinci, Improving elevated temperature performance of geopolymer concrete utilizing nano-silica, micro-silica and styrene-butadiene latex, Constr. Build. Mater. (2021), https://doi.org/10.1016/j.conbuildmat.2021.122980.
[62] M.M. Shoaib, S.A. Ahmed, M.M. Balaha, Effect of fire and cooling mode on the properties of slag mortars, Cem. Concr. Res. (2001), https://doi.org/10.1016/S0008-8846(01)00561-0.
[63] L.A. Quintero Ortiz, J. Herrera, L. Corzo, J. García, Relationship Between Compressive Strenght and Porosity Concrete Evaluated From Ultrasonic Parameters, 2011, p. 2011.
[64] S. Luhar, D. Nicolaides, I. Luhar, Fire resistance behaviour of geopolymer concrete: an overview, Buildings (2021), https://doi.org/10.3390/buildings11030082.
[65] M. Torres-Carrasco, E. Enríquez, L. Terrón-menoyo, M.J. Cabrera, D. Muñoz, J. F. Fernández, Improvement of thermal efficiency in cement mortars by using synthetic feldspars, Constr. Build. Mater. (2020) 121279, https://doi.org/10.1016/j.conbuildmat.2020.121279.
[66] E. Enríquez, M. Torres-Carrasco, M.J. Cabrera, D. Muñoz, J.F. Fernández, Towards more sustainable building based on modified Portland cements through partial substitution by engineered feldspars, Constr. Build. Mater. (2020), https://doi.org/10.1016/j.conbuildmat.2020.121334.
[67] L.D. Hung Anh, Z. Pásztory, An overview of factors influencing thermal conductivity of building insulation materials, J. Build. Eng. (2021), https://doi.org/10.1016/j.jobe.2021.102604.
[68] N.K. Lee, K.T. Koh, G.H. An, G.S. Ryu, Influence of binder composition on the gel structure in alkali activated fly ash/slag pastes exposed to elevated temperatures, Ceram. Int. (2017), https://doi.org/10.1016/j.ceramint.2016.11.042.
[69] C.L. Chan, M. Zhang, Behaviour of strain hardening geopolymer composites at elevated temperatures, Cem. Concr. Compos. 132 (2022) 104634, https://doi.org/10.1016/j.cemconcomp.2022.104634.
[70] P. Duan, C. Yan, W. Zhou, W. Luo, C. Shen, An investigation of the microstructure and durability of a fluidized bed fly ash-metakaolin geopolymer after heat and acid exposure, Mater. Des. (2015), https://doi.org/10.1016/j.matdes.2015.03.009.
[71] T. Bauer, A. Bonk, Semi-empirical density estimations for binary, ternary and multicomponent alkali nitrate–nitrite molten salt mixtures, Int. J. Thermophys. (2018), https://doi.org/10.1007/s10765-018-2456-2.
[72] D. Laing, D. Lehmann, C. Bahl, E.Z. Ag, Concrete storage for solar thermal power plants and industrial process heat, in: Conference Proceedings. Third International Renewable Energy Storage Conference (IRES 2008), 2008-11-24 - 2008-11-25, 2008. Berlin.